eman ta zabal zazu
Universidad del País Vasco
Euskal Herriko Unibertsitatea
ZIENTZIA ETA TEKNOLOGIA FAKULTATEA
FACULTAD DE CIENCIA Y TECNOLOGÍA

Bachelor Final Thesis
Degree in Physics

Optical system for low energy proton beams: Extraction, focusing and transport.

Author:
Álvaro Bermejillo Seco

Supervisor:
Iñigo Arredondo Lopez de Guereñu

Leioa, 16th June 2021

Abstract

This project performs a simulation study of the extraction, focusing and transport system of a linear particle accelerator, with special emphasis in the Low Energy Beam Transport (LEBT). First, a brief introduction to the physics of ion optics is presented. Then, SIMION, the ion optics simulation software is introduced by successfully checking a theoretical result developed beforehand. The dynamics of the beam is analysed for the system object of study, an extraction electrode, an Einzel lens and the LEBT, formed by two solenoids. The study is performed varying the magnetic field computation software. The results of emittance and beam focusing are found to be more consistent when calculated through SIMION only, than in combination with Ansys AIM. The system is found to be capable of transporting a proton beam of 30 KeV, delivering it with a radius smaller than 2 mm and a normalized RMS emittance of 0.02 mm mrad. Finally, the simulations are validated through experimental measurements of the radius of the beam, obtaining an experimental value of 1.36 mm and a simulated value of 1.22 mm.

Resumen

Este proyecto realiza un estudio mediante simulación del sistema de extracción, enfoque y transporte de haz de un acelerador lineal de partículas, con especial énfasis en el Transporte de Haz de Baja Energía (LEBT por sus siglas en inglés). Primero se presenta una breve introducción a la física de la óptica de iones. Luego se introduce SIMION, un software de simulación de óptica de iones, mediante la comprobación de uno de los resultados teóricos desarrollado previamente. La dinámica del haz es analizada para el sistema objeto de estudio, un electrodo de extracción, una lente de Einzel y el LEBT, formado por dos solenoides. El estudio se realiza variando el software de computación de campo magnético. Los resultados de emitancia y enfoque del haz resultan más consistentes cuando se calculan solo mediante SIMION, que en combinación con Ansys AIM. El sistema se encuentra capaz de transportar un haz de protones de 30 KeV, entregarlo con un radio menor a 2 mm y una emitancia normalizada RMS de 0.02 mm mrad. Finalmente, las simulaciones se validan mediante una medida experimental del radio del haz, obteniendo un resultado experimental de 1.36 mm equiparable a los 1.22 mm obtenidos mediante simulación.

Laburpena

Proiektu honek partikula-azeleragailu lineal baten izpiaren erautze, fokuratze eta garraiatze sistemak aztertzen ditu simulazio bidez, Energia Baxuko Izpien Garraioan (LEBT, ingelesezko siglen arabera) enfasi berezia eginez. Lehenik eta behin, ioien optikaren fisikari buruzko sarrera labur bat aurkezten da. Ondoren, SIMION izeneko softwarearen (ioien optika simulatzeko balio duena) sarrera labur bat egiten da, aurretik garatutako emaitza teorikoetako bat egiaztatuz. Izpiaren dinamika aztergai den sistemarako analizatzen da, sistema horren osagaiak erauzte-elektrodo bat, Einzelen lente bat eta LEBT (bi solenoide izanda) dira. Azterketa eremu magnetikoko konputatzeko software aldatuz egin da. Izpiaren emitantzia- eta fokuratze-emaitzak sendoagoak dira SIMION bidez bakarrik kalkulatzen direnean, Ansys AIMekin konbinatuta baino. Sistema 30KeVko protoi-izpia bat garraiatzeko gai da, 2 mm baino gutxiagoko erradioarekin eta 0.02mm mrad-eko RMS emitantzia normalizatuarekin entregatzeko. Azkenik, simulazioak izpiaren erradioaren neurketa esperimental baten bidez baieztatzen dira, emaitza esperimentala 1.36 mm eta simulazio bidez lortutakoa 1.22 mm izanik.

Contents

1 Introduction **1**
- 1.1 The Linac-7 project . . . 1
- 1.2 LEBT . . . 2
- 1.3 Objectives . . . 3

2 Beam characteristics **4**
- 2.1 Beam intensity . . . 4
- 2.2 Beam emittance . . . 4
- 2.3 Conservation of emittance . . . 5
  - 2.3.1 Liouville's Theorem . . . 6
  - 2.3.2 Application of Liouville's Theorem to beam dynamics . . . 6

3 Matrix formalism of ion optics **7**
- 3.1 Light optics verses ion optics . . . 7
- 3.2 Electrostatic lenses: the Einzel lens . . . 8
  - 3.2.1 The paraxial ray equation . . . 9
  - 3.2.2 Solution of the paraxial ray equation . . . 9
- 3.3 Magnetic lenses: the solenoid . . . 11
  - 3.3.1 Components of the axisymmetric magnetic field of a solenoid . . . 12
  - 3.3.2 Beam dynamics in the solenoid . . . 12
  - 3.3.3 Transport matrix for a solenoid . . . 15

4 Introduction to SIMION **16**
- 4.1 SIMION's principal characteristics . . . 16
- 4.2 Example of a simple solenoid lens simulated in SIMION . . . 17
  - 4.2.1 Focal distance of a thin solenoid . . . 17
  - 4.2.2 Focusing through a long solenoid . . . 18

5 Study of the Linac-7's LEBT **20**
- 5.1 Description of the system . . . 20
  - 5.1.1 Extraction system . . . 20
  - 5.1.2 LEBT's solenoids . . . 21
- 5.2 Characterization of the beam at the LEBT inlet . . . 23
  - 5.2.1 Particle group definition . . . 23
  - 5.2.2 Measurements of beam radius, trace-space diagram and emittance . . . 23
- 5.3 Characterization of the beam at the LEBT outlet . . . 26
  - 5.3.1 Experimental fields . . . 27
  - 5.3.2 Designed fields . . . 29

6 Experimental validation of the LEBT's focusing **31**

7 Conclusions **33**
- 7.1 Future work . . . 34

1 Introduction

As of 2007 there were more than 24,000 particle accelerators in the world [1]. At the present time, there are around 35,000 [2]. Their applications range from the well known high energy accelerators for research, to medical applications such as radiotherapy or industrial applications such as ion implanters and surface modification [2]. This huge applicability encounters an impediment, the high complexity and costs of manufacturing such devices.

1.1 The Linac-7 project

In order to go beyond this obstacle, the University of the Basque Country, in cooperation with the industry sector of the Basque Country, launches in 2018 the Linac-7 project[1]. Its main objective is the design and manufacture of a new generation, compact, robust and economic low intensity linear proton accelerator. At the same time, this project fulfills many purposes:

1. Constitute an expert research team that grows designing and manufacturing components, and integrating them into a new generation particle accelerator.
2. Generate knowledge, in the local area, in the field of particle accelerators and promote the basque industry to a competitive level in the international frame of particle accelerators.
3. Maximize the commercial use of the research and experimentation results.

The project is still in its early stages, but big part of the design process has already been conducted. The project's name gives the first information about the systems characteristics. Linac stands for Linear Accelerator and 7 makes reference to 7 MeV, which is the final energy the particles will attain. In particular, Linac-7's objective is to design a compact, low current, linear proton accelerator. In order to achieve such a design, the system is split into different stages which are designed successively, from the source of the particles, to the final accelerating stage. Linac-7 is divided into six stages: 1) ECRIO (Electron Cyclotron Resonance Ion Source), 2) LEBT (Low Energy Beam Transport), 3) RFQ (Radio Frequency Quadrupole), 4) MEBT (Medium Energy Beam Transport), 5) final accelerating element (not yet designed) and 6) beam stop.

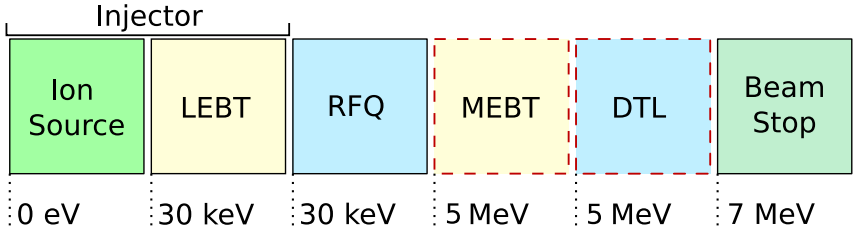

Figure 1: *Schematic description of the different stages of the Linac-7. The MEBT and the final accelerating stage, the Drift Tube Linac (DTL), are boxed in a red dashed line to indicate they have not yet been designed.*

[1]The information about the Linac-7 project is taken from internal reports. It is not available online. For consultation contact the author.

This text will focus its attention in the second of these stages: the Low Energy Beam Transport system.

1.2 LEBT

The LEBT of any particle accelerator is the stage which receives the particle beam from the ion source and delivers it to the first acceleration stage. Its purpose is not to increase the energy of the particles, but rather to shape the beam and deliver it in a suitable form for acceleration.

LEBTs can be formed with elements which are classified into two types: electrostatic and magnetic.

1. **Electrostatic lenses.** These lenses modify the trajectories of the ions by means of electric fields. Some examples are the Einzel lens [3] (Figure 2a), a group of circular electrodes with alternate high and low voltages, and the Garbor lens [4] (Figure 2b), which takes advantage of the electric field generated by an electron cloud to focus the beam.

(a) *Example of a 3 electrode Einzel lens. (Source: Purdue University.)*

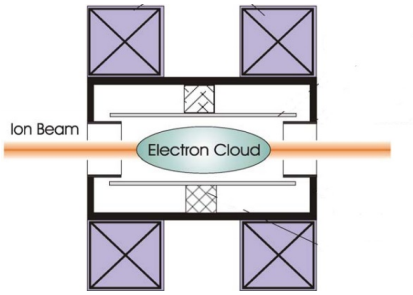

(b) *Example of a Garbor lens [4].*

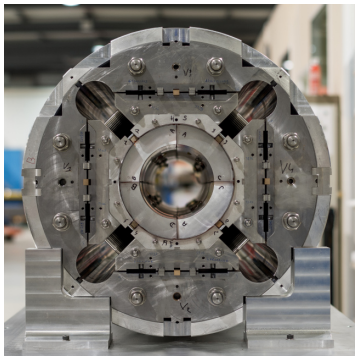

(c) *Example of a magnetic quadrupole. (Source: CERN.)*

Figure 2: *Types of lenses that form beam focusing systems.*

2. **Magnetic lenses.** These systems modify the characteristics of the ion beam by means of magnetic fields. Some examples are magnetic quadrupoles, formed either of permanent magnets or electromagnets (Figure 2c), and solenoids.

The Linac-7 design comprises an extraction electrode and a three electrode Einzel lens for the extraction of the ions from the ion source. Its aim is to give the particles from the ion source a first acceleration and make an initial focusing of the beam. The design of this piece has a huge impact in the beam dynamics, as will be discussed in a posterior section.

The LEBT's components are chosen following the required characteristics of the Linac-7 project. The more common option in the international installations is a configuration of two solenoids [5]. For the MEBT, conversely, it is more frequent to use magnetic quadrupoles due to their greater beam bending strength. With this choice, the research

group of the University of the Basque Country will be able to learn about both kinds of elements. Also, the solenoid implementation has some advantages for this particular case, as it allows a more compact design and leaves space for beam diagnostics.

For clarity, it is remarked that the extraction electrode and the Einzel lens are not part of the LEBT. The extraction system and the LEBT are differentiated stages, which can be jointly referred to as the injector. The injector is a more generic way of addressing the system which takes the particles from the source and *injects* them into the first acceleration stage, in Linac-7's case, the RFQ.

1.3 Objectives

The purpose of this text is to study and analyse the dynamics of a proton beam in the designed extraction, focusing and transport system for the Linac-7.

First, a brief introduction to the matrix formalism of ion optics will be presented. This formalism, together with the paraxial ray equation, provides an intuitive understanding on how an ion beam is focused. The aim is to obtain simple analytical equations that describe the elements present in the Linac-7: the Einzel lens and the solenoids.

Particle accelerators are complex instruments and are extremely difficult to design and study through analytical means. In order to obtain a realistic description of such systems computer simulations are very useful. In this project, we will perform simulations of the extraction and focusing system of the Linac-7 with special emphasis in the solenoids that constitute the LEBT. In relation to these simulations the following objectives are pursued:

1. **Learn how to perform ion optics simulations in SIMION** [6]. The simulations performed in this project will be carried out in the SIMION software package. It allows to calculate a system's electrostatic and magnetic fields, and simulate ion trajectories in order to study the behaviour of a beam in said system.

2. **Characterize the beam at the entry of the LEBT.** This project will not study in depth the dynamics of the beam in the Einzel lens. However, a simulation of the beam traveling through the lens with a given initial distributions of particles will be performed.

3. **Study of the Linac-7's LEBT.** Multiple simulations of the beam trajectory through the LEBT will be performed. The magnetic field generated by the solenoids will be obtained through three different methods: direct calculation in SIMION, finite elements in Ansys AIM [7] and adapted simulation in Ansys AIM through comparison with experimental data. Results of the emittance, trace-space diagrams and focusing of the beam at the entry of the RFQ will be compared.

Finally, we will take experimental data of the focusing of the beam for a given configuration of the Einzel lens and current of the solenoids. That data will be compared with the results obtained through simulation in order to corroborate the validity of the methodology followed in the simulations.

2 Beam characteristics

In order to describe an ion beam, some measurable quantities need to be defined. In the case of a LEBT there are two important qualities of the beam which need to be described:

1. How many and how fast do protons travel through the system, which will be given by the intensity of the beam.
2. The width, divergence and dispersion of the beam, which will be given by the trace-space diagram and emittance of the beam. The latter is usually referred to as a quality factor of the beam [8, 10].

Each of these quantities have different definitions based on the particular necessities of each kind of particle accelerator, so it is important to define them rigorously.

2.1 Beam intensity

Intensity is defined in the usual way, same as in a metallic conductor for electrons, and measured in amperes [8].

$$I = qN_p \tag{2.1}$$

N_p being the average number of particles that cross an area per unit time and q the electric charge of the particles. There are other ways of defining the intensity which make more sense after the acceleration section. Those definitions take into account that the beam comes in particle bunches according to the frequency of the RQF. This is not the case in the LEBT of an accelerator [8].

The intensity of a beam is usually measured with a Faraday cup [9].

2.2 Beam emittance

The emittance provides a quantitative basis for describing the quality of an ion beam. It is closely related to two-dimensional projections of the volume occupied by the ensemble of particles in six-dimensional phase-space, as defined by the set of canonical coordinates, positions and moments (q, p). The phase-space diagram usually takes the form of an ellipse, though not necessarily, as will be seen later in this text. In practice, it is more conventional to work with the trace-space. The trace-space is formed with pairs of position and slope of the trajectory in a given plane. For the rest of this text we place the z axis over the beam propagation axis. Then, the trace-space projection over the XX' plane is formed with pairs $(x,\ x' = dx/dz)$. In this projection, the emittance can be defined as the area enclosed by the plot of x against x' of all the particles of the beam.

In Figure 3 we can see a scheme of the evolution of the trace-space diagram when traveling through a LEBT. The trace-space diagram gives information about the convergence or divergence of the beam, and through the enclosed area, the emittance of the beam. It is seen how the evolution lets the particle distribution to change, but the density of points and the area are preserved.

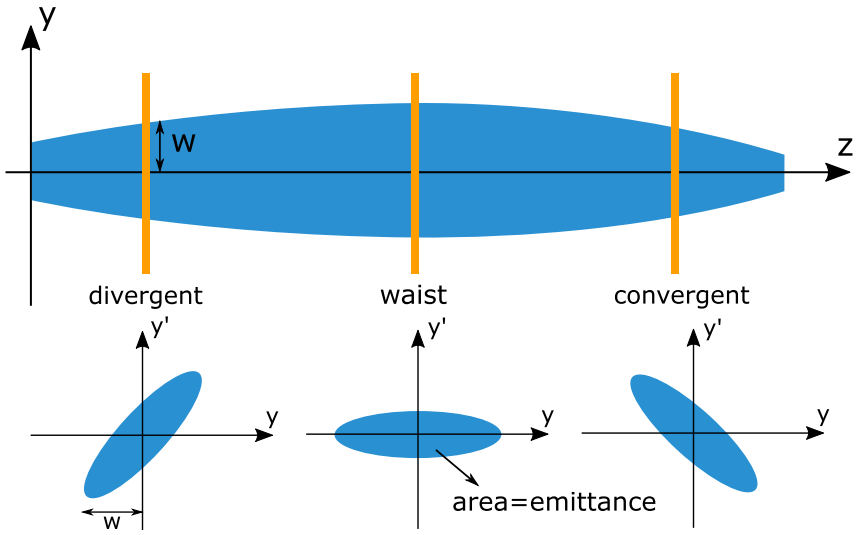

Figure 3: *Schematic evolution of the convergence of a beam going through a LEBT with the respective trace-space diagrams. It can be seen how the emittance, in a simple model the area in the trace-space diagram, is conserved in the process.*

Nevertheless, there is a more general definition of the emittance, for an arbitrary particle distribution, that is called RMS emittance [8, 10].

$$E_{xx',rms} = \sqrt{\overline{x^2}\ \overline{x'^2} - \overline{xx'}^2} \tag{2.2}$$

where $\overline{x^2}$, $\overline{x'^2}$ and $\overline{xx'}^2$ are the second central moments, or variances (as before, $x' = dx/dz$). This definition of emittance is unnormalized, which means that it changes when the momentum of the beam changes. For that reason, the normalized emittance is defined [8, 10].

$$E^N_{xx',rms} = \beta\gamma E_{xx',rms} \tag{2.3}$$

With $\beta = v/c$ and γ the Lorentz factor. The RMS definition of the emittance does not match the more vague definition given before (the area in trace-space), but in the simplest cases. For example, if the dynamics of the beam is non-linear, the RMS emittance grows while the area in trace-space remains constant.

There is not a fixed agreement in which units to use for this quantity. We will adopt the more commonly used, which is mm mrad [11].

The emittance can be measured in several ways. In this project a pepper-pot method is used [12].

2.3 Conservation of emittance

The normalized emittance of a beam remains constant along the whole accelerator and it is determined at the extraction section. Said conservation law is derived from Liouville's Theorem. This section will give a brief description of the theorem's applicability to ion beam physics.

2.3.1 Liouville's Theorem

We define a 6N dimensional phase space with coordinates $\vec{q_i}$ and $\vec{p_i}$ with $i = 1, ..., N$; N being the number of particles. A set of N points in phase-space describes the configuration of the system. If we let the system evolve with time, the N points will describe N trajectories defined by the equations of motion, given by the Hamiltonian. Those trajectories in the 6N dimensional phase-space do not cross each other; for each initial condition ($\vec{q}$, $\vec{p}$) there is a unique solution of the canonical equations, derived from the Hamiltonian [13].

Liouville's Theorem states that if a distribution of points in phase-space is described by a density function $\rho(\ \vec{q},\ \vec{p}\ )$, and its motion by the canonical Hamiltonian equations, then the phase-space density is invariant.

$$\frac{d\rho}{dt} = 0 \tag{2.4}$$

2.3.2 Application of Liouville's Theorem to beam dynamics

If the particles do not interact with each other, i.e., the electromagnetic fields are external, the 6N phase-space can be reduced from 6N to a 6 dimensional space called μ-space and Liouville's Theorem still holds. In particular, and more useful in this problem, attention may be focused in one of the coordinates. By definition, $x' = dx/dz = d\dot{x}/d\dot{z} \simeq p_x/p$ ($p = |\vec{p}\ | >> p_x, p_y$)[2], so the density function (2.4) can also be defined for the trace-space, and the conservation law holds. That way, by plotting a 2 dimensional diagram ($x,\ x'$), we can visualize the emittance (broadly, the area enclosed by the outermost particles in the diagram as can be seen in Figure 3). The emittance will remain constant if the conditions of Liouville's Theorem are fulfilled and the equations of motion in all coordinates are uncoupled [8].

A charged particle beam does not strictly fulfill Liouville's Theorem as it has been described. Thus, the conservation of emittance is limited by some additional restrictions. The primary cause of emittance growth is the space-charge effect, that is, the ion-ion interaction. For phase-space volume to be conserved in the 6 dimensional μ-space, particles need to be non-interacting. If the interaction between particles becomes important, phase-space volume is conserved in the 6N dimensional space defined by ($\vec{q_i}$, $\vec{p_i}$), but not μ-space. Nevertheless, in low current particle accelerators space-charge effects are often neglected and emittance is assumed to be conserved [8]. We remark that Liouville's Theorem makes reference to the density in phase-space, so it is applicable to the conservation of the area in trace-space diagrams, but not necessarily to the RMS definition of emittance. A growth in RMS emittance does not mean that Liouville's Theorem is violated. It does mean, however, that the trace-space diagram is being distorted, and it could be undesirable from a beam design point of view [10].

The most important conclusion from this result is that the emittance has a lower boundary: the emittance at the ion source. It should not be expected to get a lower emittance by any method other than subtracting particles from the beam [14].

[2]Remember that z corresponds to the propagation axis.

3 Matrix formalism of ion optics

The description of the dynamics of a particle beam in a particle accelerator is given in a similar way to that of light beams. The different elements in the accelerator are viewed as lenses and described by a transfer matrix which operates on the vectors representing the incoming ray (particle). However, there are significant differences between light and ion optics.

3.1 Light optics verses ion optics

The principal differences between light and ion optics are the following [6]:

1. In the most simple model, light refraction occurs in the sharp transitions of light velocity when they enter a different medium. The radius of refraction changes from infinite everywhere (straight lines) except in the boundaries where it approaches zero. However, ion optics always behaves as light in non-constant index refraction mediums (e.g., air with heat gradient). This results in gradual changes of the refraction radius. This refraction results from electromagnetic forces normal to the ion's velocity

$$r_n = \frac{mv^2}{eE_n}, \qquad r_n = \frac{mv}{eB_n} \tag{3.1}$$

   Where m is the mass of the particle, v the velocity, e the electric charge, r_n the refraction radius and E_n, B_n the normal components of the electric and magnetic fields. From these simple equations it can be extracted that all particles starting at the same point, with the same direction and kinetic energy, will have identical trajectories in electrostatic (only) fields. However, for a given initial kinetic energy the trajectories will be mass dependent in magnetic fields. This is due to the fact that electrostatic r_n is proportional to the kinetic energy while the magnetic r_n is proportional to the momentum of the particle. Moreover, because of the v verses v^2 effect on the r_n, magnetic ion lenses are more refractive at high velocities. That is the reason why magnetic quadrupoles are more common in MEBTs [10].

2. Visible light optics has the advantage that its energy has little variation, from 1.84 eV for red to 3.2 eV for violet. Conversely, ions can vary their energies by any arbitrary amount, from 0 to, for example, the 6.5 TeV reached in the LHC [15].

3. Light optics can be modeled using physical optics benches. In contrast, in ion optics there is usually no access to interior beam shapes due to the necessity of vacuum chambers, only end to end measurements. This is a strong reason why computer simulations are so important for particle accelerator designing.

4. Photons are massless particles. However, ion optics is affected by the different masses, from that of the electron to those of massive atomic nuclei. This affects, not only for the lower refracting power of a given field, but also for the varying relativistic effects particles undergo. In Figure 4 the velocities as function of the kinetic energy of an electron and a proton are shown. It can be noticed that, for example, for the energies of our project (30 KeV just after the source) the electron

would have appreciable relativistic effects, whereas for the proton or heavier nuclei they can be ignored.

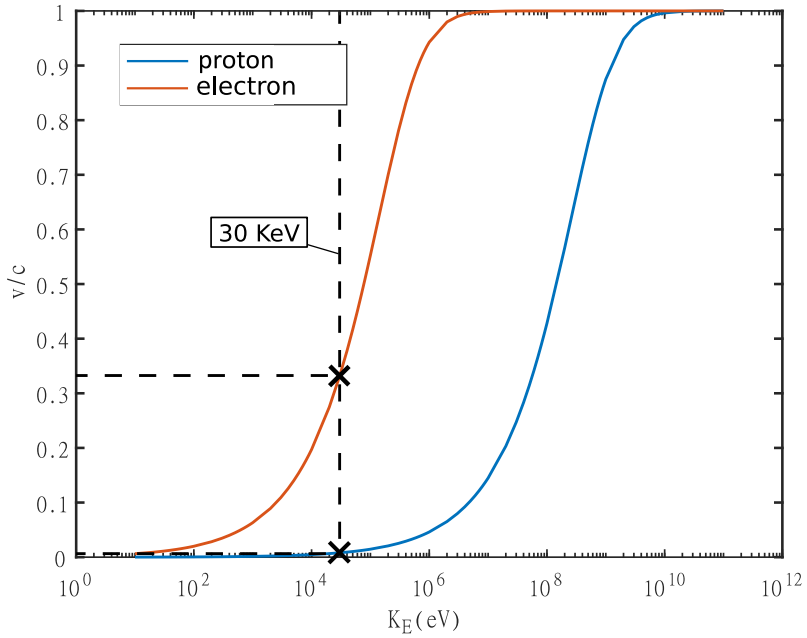

Figure 4: *Velocity of the electron and the proton as a function of their kinetic energy.*

3.2 Electrostatic lenses: the Einzel lens

Linac-7's ion extraction is performed by means of an extraction electrode and an Einzel lens. An Einzel lens is a set of cylindrical apertures along the beam axis with alternating high and low polarity. The electric field generated by this element can provide focusing and acceleration to charged particle beams. In particular, it is effective in the low energy ranges.

A mathematical description of the Einzel lens is found in the frame of ion optics using the standard matrix formalism of magnetic ion optics [3]. In a system with cylindrical rotational symmetry as ours, we can define a ray vector for an arbitrary charged particle at any specified position along the axis of propagation z.

$$\vec{r}(z) = \begin{pmatrix} r \\ r' = dr/dz \end{pmatrix} \begin{pmatrix} \text{radial displacement} \\ \text{radial angle deviation} \end{pmatrix} \tag{3.2}$$

Thus, the transformation of the ray coordinates by an ion optical system is represented by a 2×2 matrix R(z), called transport matrix. To calculate the components of the transport matrix we will have to solve the paraxial ray equation, which will be deduced hereafter. The paraxial approximation is a first order approximation, which makes all calculations valid only for small angles, that is, near the axis of propagation.

3.2.1 The paraxial ray equation

The starting point is Newton's equation of motion $\frac{d}{dt}\vec{p} = -e\vec{\nabla}V$ whose components may be written [3]

$$\frac{d}{dt}(\gamma m\dot{r}) = -e\frac{\partial V}{\partial r}, \qquad \frac{d}{dt}(\gamma m\dot{z}) = -e\frac{\partial V}{\partial z} \tag{3.3}$$

Where V is the electric potential, γ the Lorentz factor and dots represent time derivatives. Replacing the time variable by the traversed distance z,

$$v_z = \dot{z} = \frac{dz}{dt}, \qquad \frac{d}{dt} = v_z\frac{d}{dz} \qquad \Longrightarrow \qquad \dot{r} = v_z r' \tag{3.4}$$

With these changes, (3.3) can be written in the following way, which is the paraxial ray equation

$$r'' = \frac{e}{\gamma m v^2}\left(r'\frac{\partial V}{\partial z} - \frac{\partial V}{\partial r}\right) \tag{3.5}$$

To derive the first order paraxial ray equation the potential is expanded in a power series taking into account Laplace's equation in cylindrical coordinates (with rotational symmetry)

$$\frac{\partial^2 V}{\partial z^2} + \frac{1}{r}\frac{\partial V}{\partial r}\left(r\frac{\partial V}{\partial r}\right) = 0 \tag{3.6}$$

Since rotations in θ do not change the potential, all odd powers in the power series of V banish

$$V(r,z) = \sum_{n=0}^{\infty} A_n(z) r^{2n} \tag{3.7}$$

Introducing (3.7) into (3.6) the following result is obtained,

$$V(r,z) = V(0,z) - \frac{r^2}{4}V^{(2)}(0,z) + \frac{r^4}{64}V^{(4)}(0,z) + \dots \tag{3.8}$$

The exponent in parentheses represents an order of derivation with respect to z. So, introducing (3.8) to the lowest order into (3.5), the paraxial equation in the non-relativistic ($\gamma = 1$) linear approximation reads

$$r'' = \frac{e}{pv}\left(r'V'(z) + \frac{r}{2}V''(z)\right) \tag{3.9}$$

3.2.2 Solution of the paraxial ray equation

The central element of electrostatic ion optics is called accelerating tube lens (Figure 5). An approximate solution to equation (3.9) for the potential of the accelerating tube is $\vec{r}(z_2) = R\,\vec{r}(z_1)$, where R is the following transfer matrix [3]

$$R = \begin{pmatrix} 1 & 0 \\ \frac{E_2 - E_1}{2p_2v_2}\frac{1}{L} & 1 \end{pmatrix}\begin{pmatrix} 1 & L_{\text{eff}} \\ 0 & \frac{p_1}{p_2} \end{pmatrix}\begin{pmatrix} 1 & 0 \\ \frac{E_1 - E_2}{2p_1v_1}\frac{1}{L} & 1 \end{pmatrix} \tag{3.10}$$

where E stands for total energy (T+V). The indices 1 and 2 make reference to the initial

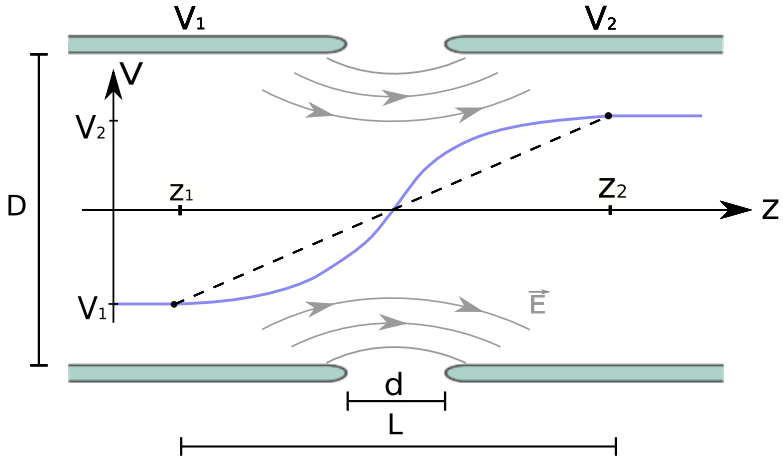

Figure 5: *Scheme of an accelerating tube lens. V_1 and V_2 are the potentials with respect to the ion source. The electric field $\vec{E}$ acts as a focusing lens at the entrance and as defocusing at the exit. The distance L, between points z_1 and z_2, is approximately $D + d$, respectively, the diameter and separation between tubes. The blue line depicts the potential V(z) along the axis and the dashed line is taken as an approximation.*

and final points of the element, separated a distance L, as shown in Figure 5. The effective longitude (L_{eff}) in the center matrix, the drift matrix, is

$$L_{\text{eff}} = L\frac{p_1 c}{E_2 - E_1} ln\frac{p_2 c + E_2}{p_1 c + E_1} \tag{3.11}$$

When the particle goes through the lens with $E_2 > E_1$,which happens only if $V_2 > V_1$, the matrix is a sequence: focusing lens - drift - defocusing lens. For $E_1 > E_2$ the sequence is the opposite. Notice that in both cases the defocusing is weaker than the focusing, due to the change in the momentum of the particle.

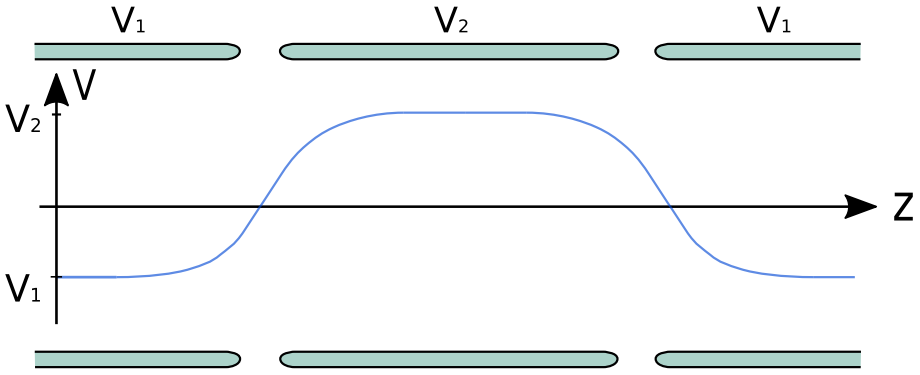

Figure 6: *Scheme of an Einzel lens. V(z) depicts the potential along the axis of propagation.*

The description of the accelerating tube allows to immediately present the transfer matrix of an Einzel lens. The scheme of an Einzel lens is shown in Figure 6. It consists of two acceleration tubes from V_1 to V_2 and back to V_1. So the transport matrix for the whole lens reads [3],

$$R = R(V_1, V_2)R(V_2, V_1) \tag{3.12}$$

The most simple Einzel lens is formed by two accelerating tubes, but there is no limit to its number.

3.3 Magnetic lenses: the solenoid

A solenoid is a type of electromagnet, a cylindrical coil which creates a magnetic field when carrying an electric current. The definition of a solenoid is simple, but their design can be of high complexity.

The magnetic flux density field of a solenoid is very characteristic. It is very constant in the inner region of the cylinder and decays rapidly out of it. The typical profile of the magnetic field along the axis of revolution of a solenoid is shown in Figure 7a and the contour of the field in a section perpendicular to the axis in Figure 7b. The contour shows how the field is more intense in the region near the conductors and reaches a minimum in a point in the center of the circle. The line formed by all those minimum field points from all the sections of the solenoid make up the magnetic axis.

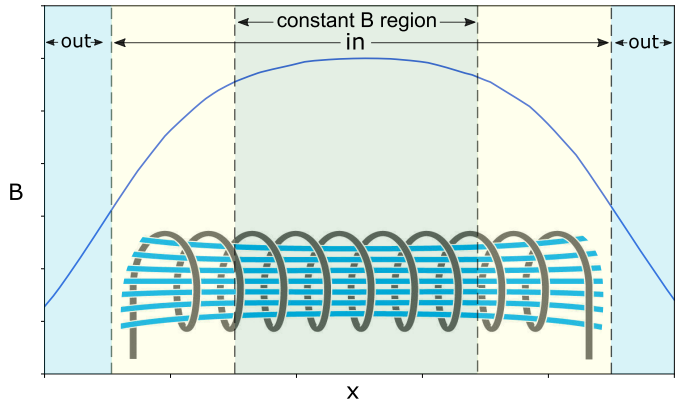

(a) *Example of the magnetic flux density amplitude along the axis of a solenoid. Three regions: outside of the solenoid, inside of the solenoid and in green the constant B region of the solenoid. Arbitrary units.*

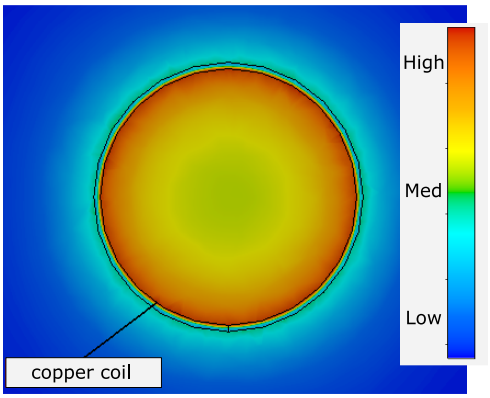

(b) *Example of the magnetic flux density contour in a section perpendicular to a solenoids axis. It can be appreciated how the field is weaker in the center, along the magnetic axis. Arbitrary units.*

Figure 7: *Characteristic magnetic field of a solenoid. Computed in Ansys AIM.*

Solenoids are the most common focusing and transport systems for low energy particle beams [5]. It is not obvious, though, why the uniform magnetic field of a solenoid produces this focusing. It is frequent to picture helical trajectories with a constant radius, getting the impression that no focusing happens at all. In this section, a simple model is developed to analyse its origin. Also, the trajectories of charged particles going through a solenoid will be examined.

This model requires from the following assumptions [16]:

1. Coulomb repulsion between particles is ignored (charge force effect).

2. The beam is assumed to be cylindrical, uniform and with no initial transverse velocity (cold beam).

3. The magnetic field of a solenoid is simplified. It is assumed to be longitudinal and uniform inside the solenoid, from 0 to L (the length of the solenoid), and zero outside.

3.3.1 Components of the axisymmetric magnetic field of a solenoid

First, the components of the axisymmetric magnetic field of a solenoid need to be calculated in order to apply the paraxial approximation [17]. The starting point is Laplace equation (3.6) for the magnetic scalar potential (Ψ). In the region around $r = 0$ the magnetic scalar potential can be used due to the absence of electric currents $\vec{J} = 0$, magnetic field lines do not close in this region. Which means that $\nabla \times \vec{H} = 0$, from where $\vec{H} = -\nabla\Psi$. The relationship between the magnetic field and the scalar potential is analogous to the usual in electrostatics [17],

$$B_z = -\mu\frac{\partial\Psi}{\partial z}; \qquad B_r = -\mu\frac{\partial\Psi}{\partial r} \tag{3.13}$$

Finally, from (3.8) for the magnetic scalar potential and (3.13) we obtain the axisymmetric magnetic field of a solenoid

$$\begin{aligned} B_z(r,z) &= B(z) - \frac{r^2}{4}B^{(2)}(z) + \frac{r^4}{64}B^{(4)}(z) + \dots \\ B_r(r,z) &= -\frac{r}{2}B^{(1)}(z) + \frac{r^3}{16}B^{(3)}(z) + \dots \end{aligned} \tag{3.14}$$

In the paraxial approximation only terms to first order in r are kept. Thus, taking into account the description of the magnetic field given in the assumptions, the magnetic field is

$$B_z(r,z) = B_0\left[\Theta(z) - \Theta(z-L)\right], \qquad B_r(r,z) = -\frac{r}{2}B_0\left[\delta(z) - \delta(z-L)\right] \tag{3.15}$$

where B_0 is the magnetic flux density field amplitude inside the solenoid, Θ the Heaviside function and δ the Dirac delta function.

3.3.2 Beam dynamics in the solenoid

To discuss the dynamics, space is divided into sections [16]. There are 3 differentiated sections: region I $\rightarrow [z < 0]$, region II $\rightarrow [0 < z < L]$ and region III $\rightarrow [L < z]$. In regions I and III, which have no fields, the trajectory of a charged particle is a straight line, while in section II it is helical due to the constant magnetic field. In the boundary between regions I and II the radial magnetic field is a Dirac delta function, so it gives an impulse in a perpendicular direction: the azimulthal direction. The force is given by

$$F = q\vec{v} \times \vec{B} = ev_z B_r(z)\hat{\theta} \tag{3.16}$$

with v_z the initial velocity of the particle along the longitudinal axis.

To compute the change in velocity due to that transition, it is useful to take into account conservation of canonical angular momentum, a direct application of Noether's Theorem [20]. This conservation law is a consequence of the system's continuous symmetry to any rotation $\delta\theta$ about the z axis. The canonical angular momentum (3.17) is derived from the Lagrangian of a charged particle in a magnetic field.

$$P_\theta = [\vec{r} \times (\vec{P} + \frac{e}{c}\vec{A})] \cdot \hat{z} \tag{3.17}$$

where $\vec{A}$ is the potential vector, $\vec{P}$ the momentum of the particle (γmv) and c the speed of light. From $\vec{B} = \nabla \times \vec{A}$ we can derive the potential vector for the solenoid (not unique) [20]

$$\vec{A} = A_\theta \hat{\theta} = \frac{1}{2} B_0 r \hat{\theta} \tag{3.18}$$

Hence, the canonical angular momentum for this specific problem is

$$P_\theta = m\gamma r v_\theta + \frac{e}{2} B_0 r^2 \tag{3.19}$$

The conservation of this quantity is known as Busch's theorem [20]. Outside the solenoid, $B_z = 0$ and $v_\theta = 0$, so $P_\theta = 0$. In order to conserve that quantity, inside the solenoid the particle attains an azimuthal velocity

$$\Delta v_\theta = -\frac{eB_0}{2\gamma m} r_0 \tag{3.20}$$

where r_0 is the coordinate of the particle when it enters the solenoid. In this frame, the cyclotron (ω_c) and Larmour (ω_L) frequencies are defined as

$$\omega_c = \frac{eB_0}{\gamma m}, \qquad \omega_L = \frac{\omega_c}{2} = \frac{eB_0}{2\gamma m} \tag{3.21}$$

We can therefore write $\Delta v_\theta = r_0 \omega_L$. The cyclotron frequency describes how rapidly the particle rotates around the axis of its own trajectory. The Larmour frequency, instead, is the angular velocity about the axis of the solenoid [16]. The particle will, then, describe a helical trajectory of radius

$$R_c = \frac{\gamma m |v_\theta|}{eB_0} = \frac{r_0}{2} \tag{3.22}$$

which crosses periodically through the axis of the solenoid (Figure 8).

To describe what happens at the boundary between regions II and III, the trajectories of the particles in region II are studied in more detail. The radial and azimuthal coordinates are given by

$$r = r_0 \cos\left(\frac{\omega_L z}{v_z}\right), \qquad \theta = \theta_0 + \frac{\omega_L z}{v_z} \tag{3.23}$$

and the particle velocity, taking the derivatives in (3.23), are

$$v_r = -r\omega_L \tan\left(\frac{\omega_L z}{v_z}\right), \qquad v_\theta = r\omega_L \tag{3.24}$$

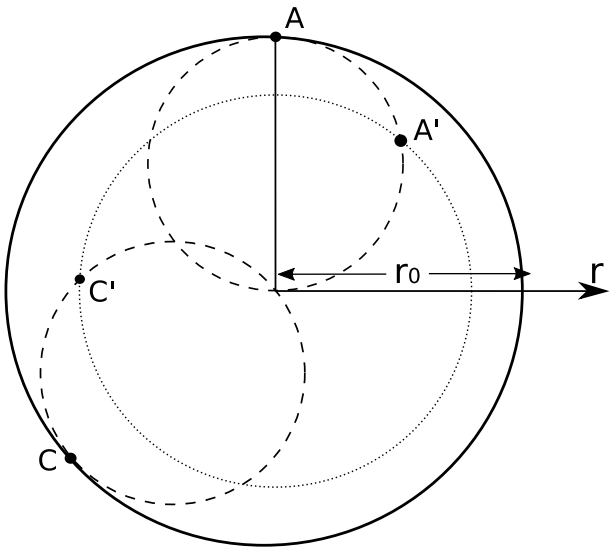

Figure 8: *Pictorial explanation of the periodic focusing of a particle beam in a solenoid. The solid circumference shows the border of the beam when it enters the solenoid. The dashed lines show the trajectories of individual electrons. After the beam travels some time through the solenoid electrons from the periphery $r = r_0$ (A and C) are more proximate to the axis (A' and C'). The border of the beam is now the dotted line and the beam is thus focused. Notice that after some time the beam will return to its original shape (A' and C' will travel to A and C) [16].*

As can be seen in Figure 9, the coordinates (r, θ) are measured relative to a point O in the solenoid axis.

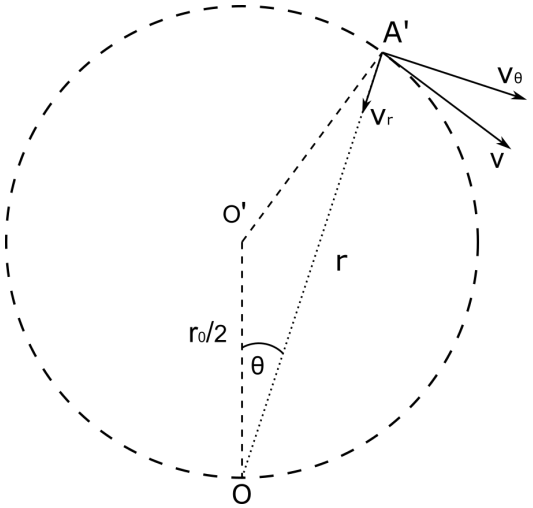

Figure 9: *Radial an azimuthal components of the particle's velocity with respect to the solenoid axis O in point A'. O' is the axis of the particle's trajectory [16].*

In the boundary between regions II and III, v_θ undergoes a sudden change in the opposite direction as in the previous boundary (3.20)

$$\Delta v_\theta = r_1 \omega_L \tag{3.25}$$

Looking at (3.24) and (3.25), from $z = L$ onwards $v_\theta = 0$. However, the radial velocity

remains unchanged at the boundary

$$v_r = -r_1 \omega_L \tan\left(\frac{\omega_L L}{v_z}\right) \tag{3.26}$$

In region III there is no magnetic field, so the particle follows a straight trajectory. And, assuming that the tangent in (3.26) is positive, after the beam undergoes a periodic focusing inside the solenoid due to the helical trajectory, each particle attains a radial velocity towards the axis of the solenoid. Ideally, the beam will be focused after traveling a distance

$$z = L + \frac{v_z}{\omega_L} \cot\left(\frac{\omega_L L}{v_z}\right) \tag{3.27}$$

3.3.3 Transport matrix for a solenoid

An equivalent transport matrix to that of the Einzel lens can be computed for the solenoid. The transport matrix of an element given its focal length is given by [20]

$$R = \begin{pmatrix} 1 & 0 \\ -\dfrac{1}{f} & 1 \end{pmatrix} \tag{3.28}$$

and the focal distance of a solenoid in the approximation of thin lens ($v_z/\omega_c << L$) is [17]

$$\frac{1}{f} = -\frac{r'}{r} = \frac{e^2 B_0^2 L}{4\gamma^2 m^2 v_z^2} \tag{3.29}$$

where $r' = dr/dz$ and r is as given in (3.23).

4 Introduction to SIMION

To analyse in detail the behaviour of ions going through the injector, computer simulations are helpful. In this project SIMION 8.1 will be used to perform these simulations. SIMION is an ion optics simulation program that models ion optics problems with 2D symmetrical and/or 3D asymmetrical electrostatic and/or magnetic fields. This section will introduce some of the principal characteristics of this software package, and perform some simple simulations in order to get familiarised and validate some of the analytical results developed in Section 3.

4.1 SIMION's principal characteristics

SIMION is a very complete and complex ion optics simulation program with many functionalities. The principal characteristics that have been used for the purposes of this project are presented hereafter [6].

1. **Workbench.** SIMION's simulation universe is an $8km^3$ cubic volume. In that universe the user defines an Ion Optics Workbench, which is an imaginary 3D rectangular volume within the simulation universe where the simulations are conducted. Anything defined in a given simulation is specified in the workbench.

2. **Potential Array.** SIMION utilizes potential arrays to define electrostatic and magnetic fields. A potential array is an array of points organized in square (2D) or cubic (3D) grids set in a given region of the workbench. All points have a potential and a type (electrode or non-electrode). The electrode points create the boundary conditions for the array. Given a grid with electrode and non-electrode points, Laplace equation is solved to obtain the potentials of the non-electrode points.

3. **Geometry File.** In order to calculate the potential array of a given system, first the geometry has to be defined. That is, the user has to define the region in which there will be an electrostatic or magnetic field, specify the position and geometry of the electrodes and introduce any symmetry of the system (planar or cylindrical).

4. **Particle definition.** Another important step is the definition of the particle group that forms the beam. SIMION enables various ways of defining it. The easier is the FLY2 format, which allows, through the interface, to define the mass, initial kinetic energy, velocity direction and distribution of a group of particles.

5. **User programming.** The functionality with most potential is the user programming in the programming language Lua [18]. It enables to access many of the variables of the simulations. For example, it gives the possibility of calculating the magnetic flux density field generated by a current through the Biot-Savart law, or allows to introduce externally computed magnetic fields. Moreover, it is through user programs that the positions and velocities of the particles can be recorded in order to extract information, such as the emittance or the beam loss[3].

[3]Beam loss is a characteristic of any element in an accelerator. It can be defined as the percentage of particles present at the entrance of an element that are not present at the exit of said element.

4.2 Example of a simple solenoid lens simulated in SIMION

To introduce the use of SIMION we will perform a simulation of the focusing of a proton beam when traveling through a simple solenoid. From that simulation we will extract the focal distance and compare it with an analytical approximation extracted from equation (3.29).

4.2.1 Focal distance of a thin solenoid

To set this simulation up we need to select the following parameters: radius, length, number of turns and current that flows through the solenoid, the kinetic energy and distribution of the protons. The radius and length of the solenoid are chosen to be 10 mm and 20 mm respectively. The number of turns and current of the solenoid are adjusted at the same time as the kinetic energy of the protons so that the thin lens approximation is valid. With 50 turns and a current of 7 A the measured magnetic field in the centre of the solenoid is 15.5 mT. Setting the kinetic energy of the proton at 50 eV ($v \simeq 98 \cdot 10^3$ m/s results in the following thin lens parameter

$$\frac{v_z}{\omega_c} = 0.13 \tag{4.1}$$

which is approximately 7 times bigger than the length of the solenoid. It is not pursued to obtain a better fulfillment of the thin lens approximation, because if the velocity of the particles is increased, the focal length increases as v^2 and it is more difficult to extract a measurement from the simulation. Decreasing the magnetic field also increases the parameter, but has the same effect as velocity changes. The focal length is thus computed through (3.29).

$$f = \frac{4m^2 v_z^2}{e^2 B^2 L} = 0.902\ m \tag{4.2}$$

The results obtained from the simulation are shown in Figure 10. In order to compute the focal distance through simulation, the protons are created in a circle distribution and with a velocity parallel to the z axis (as coming from the infinite). In this manner, the protons cross the z axis in the focal point. The result is $f = 0.918$ m. Thus, the calculation performed though the thin lens approximation commits a relative error of 1.74 % with respect to the simulation result.

If we analyse the projection of the particle trajectories over the plane perpendicular to the z axis shown in Figure 10, some of their characteristics described in Section 3.3.2 can be noticed. Every trajectory starts as a red point, indicating a trajectory parallel to the z axis. The change of colour of the trajectory from red to green marks the entry of the particles into the magnetic field of the solenoid. At that that point, the particle starts to rotate, following the typical helical trajectory of a charged particle in a magnetic field. When they come out of the magnetic field region of the solenoid they become red again and follow a straight line corresponding to the dynamics of a particle to which no forces are applied. In the process of going through the solenoid, each particle attains a radial velocity which makes the beam become focused at a 0.918 m distance from the centre of the solenoid.

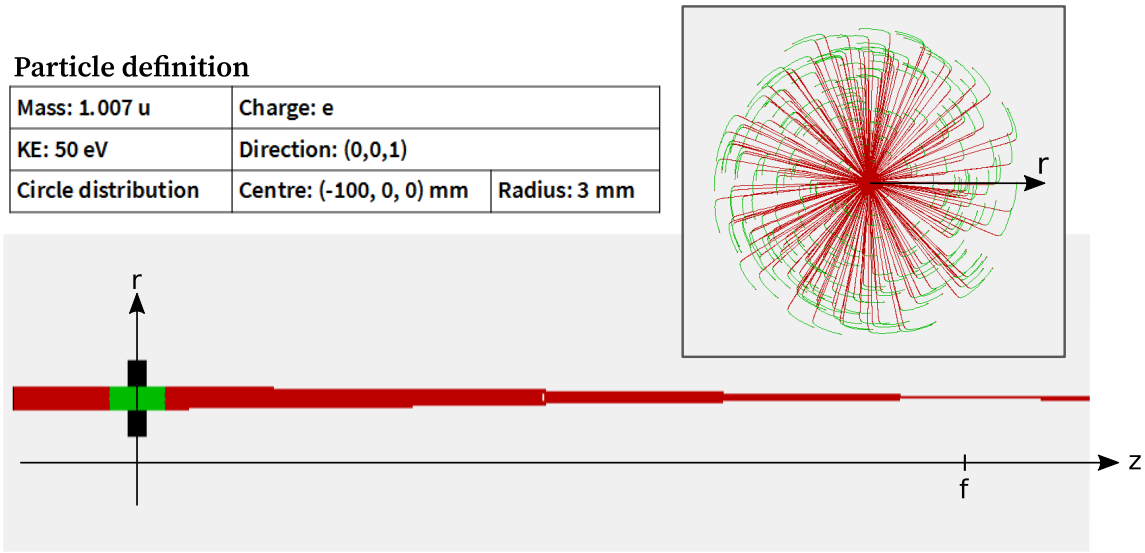

Figure 10: *Results from the simulation performed for the focusing of a circular distribution particle group starting with velocity parallel to the z axis. The table indicates the parameters of the particle group (u stands for atomic mass unit). The projection of the trajectories over two planes are shown. The trajectory of any particle changes color from red to green when it enters a region with $B > 0.9$ mT. The focal distance is found to be 0.918 m.*

4.2.2 Focusing through a long solenoid

It is interesting to analyse the behaviour of the dynamic of a beam when the thin lens approximation ceases to be valid. The configuration of the system is, then, adapted by making the solenoid longer (480 mm) and increasing the magnetic field inside the solenoid by setting a current of 8 A and a winding of 1500 turns. In this configuration the magnetic field inside the solenoid has a very constant value of 31.3 mT.

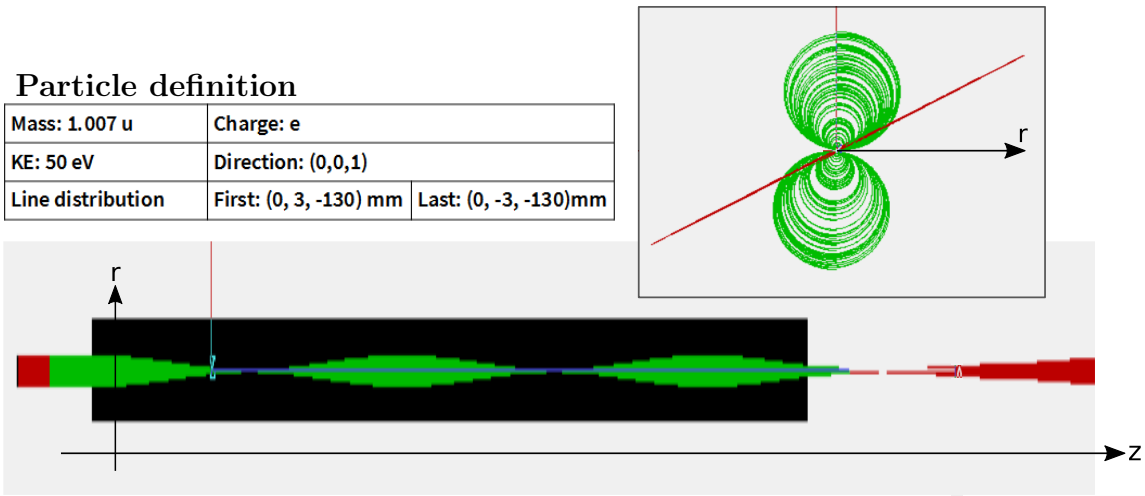

Figure 11: *Results from the simulation performed for the focusing of a linear distribution particle group starting with velocity parallel to the z axis. The table indicates the parameters of the particle group. The projection of the trajectories over two planes are shown. The trajectory of any particle changes color from red to green when it enters a region with $B > 0.9$ mT. The beam experiments a periodic focusing before going out of the solenoid.*

The thin lens parameter for this system takes a value of 0.033. So, in this case the thin lens approximation is not valid because L is 14.7 times greater than v_z/ω_c. The result of this simulation can be inferred from the analysis shown in Section 3.3.2, and particularly from Figure 8. When L/v_z is greater than $2\pi/\omega_c$, each particle has enough time to give more that 1 loop in its helical trajectory inside the solenoid. Thus, the beam is periodically focused with period $2\pi/\omega_c$. This expected behaviour can be observed in Figure 11.

We can see how the beam is focused three times along its trajectory, two inside the solenoid and one last time outside of it. If we focus our attention in the projection over the plane perpendicular to the z axis, the cyclical trajectories can be noticed. The initial distribution of the particles is a vertical line. When they enter the magnetic field, they start their helical trajectories with centre in $r_0/2$, r_0 being their radial coordinate when entering the solenoid. They perform nearly two and a half loops and then diverge after the final focusing. That diverging is presented here in the inclined red line, which corresponds to the particles following a straight trajectory.

5 Study of the Linac-7's LEBT

In this section we will perform a complete simulation of the injector of the Linac-7. First, we give a description of the system's geometry and electrostatic/magnetic fields.

5.1 Description of the system

The system has the structure shown in Figure 12. Its is divided into two main structures, the extraction system and the LEBT, which are explained in detail in this section.

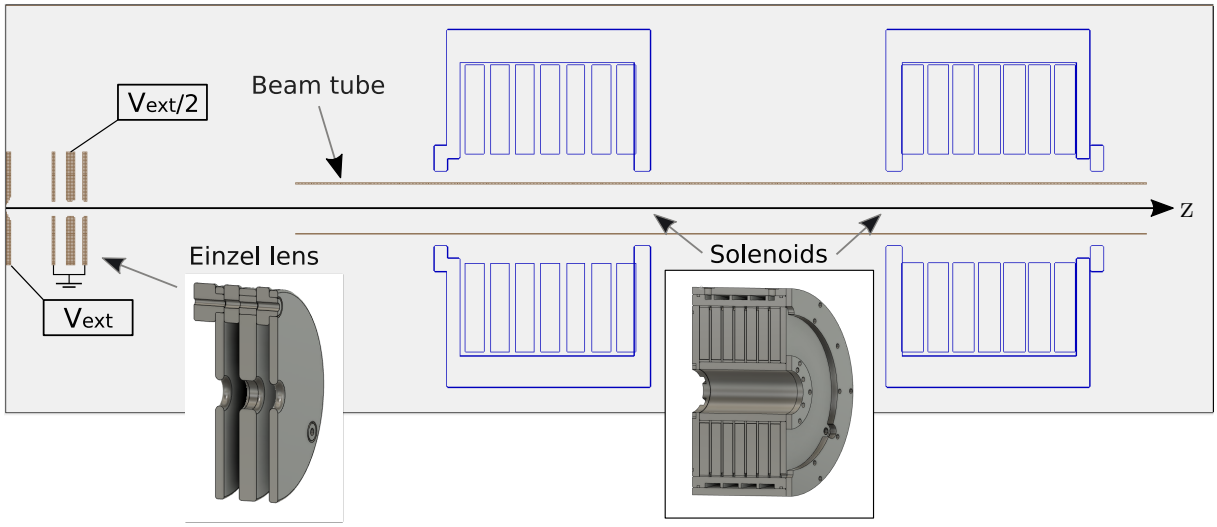

Figure 12: *Layout of the injector as it appears in SIMION. From left to right: extraction electrode, Einzel lens (its centre electrode at half the voltage from the extraction electrode, the beam tube and the two solenoids. The 3D models of the design in Fusion360 [19] are shown for the Einzel lens and the solenoids for greater detail. Scale: length of each solenoid, 171mm.*

5.1.1 Extraction system

The extraction electrode, the first element we encounter in Figure 12, is situated after the ion source and gives the ion beam the initial increase in kinetic energy. In ion beam optics it is often referred to as aperture lens[4]. As a first approximation, this element generates a constant electric field perpendicular to its surface, accelerating the particles that come out from its aperture. In Figure 13 we can see a representation of a potential energy surface in a symmetry plane of the system, calculated in SIMION. This representation is useful to gain an intuitive idea of how the particles move through the electric field generated by any electrode system. The behaviour of charged particles traveling through that region of space is similar to how a ball would in a hill with the same slope. We can note how the particles gain kinetic energy between the extraction electrode and the first electrode of the Einzel lens. Then, the beam travels through the Einzel lens and most of the divergence acquired in the extraction electrode is compensated.

[4]This component has its associated transport matrix in the formalism described in Section 3. It is very similar to the side matrices in (3.10).

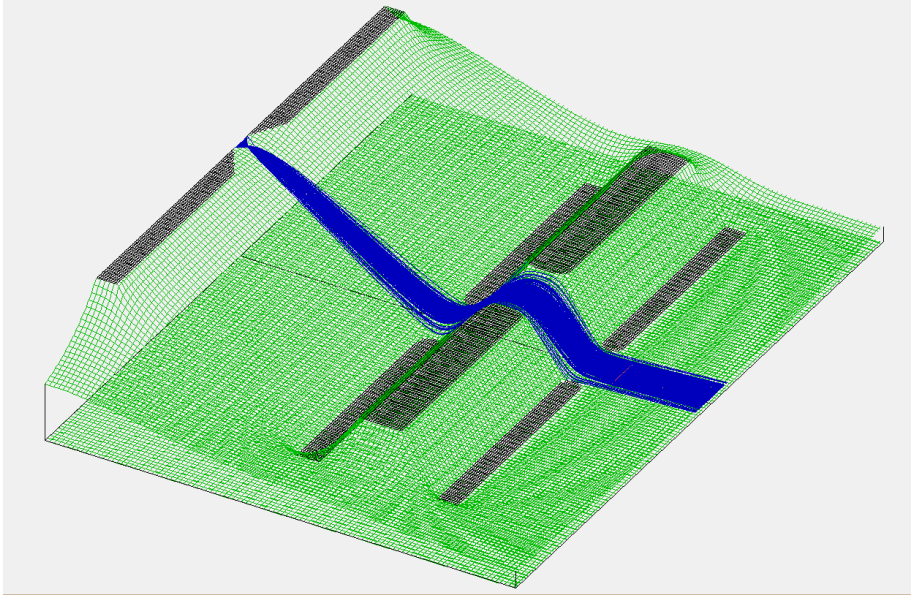

Figure 13: *PE view in SIMION. The green surface represents a potential energy surface in a mirror symmetry plane of the system. It also shows the electrodes, in black, and the blue lines are the trajectories of individual protons.*

5.1.2 LEBT's solenoids

We now describe the main element of this project, the LEBT's solenoids.

Geometry

As can be seen in Figure 14, the solenoid is assembled from several pieces. The beam tube, which is not part of the solenoid, are the walls of the region marked as 1. The rectangle marked as 2 is one of the 7 sub-coils. Those sections are where the copper wiring is placed and through where the current flows. And the region marked as number 3 is the steel casing, the element which confines the magnetic field inside the solenoids.

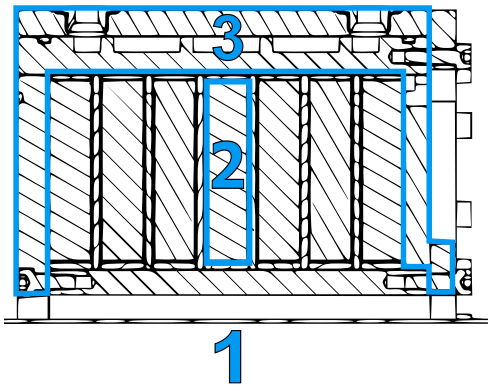

Figure 14: *Scheme of the solenoid where the different components can be differentiated. 1) Aluminium beam tube. 2) Copper wiring section. 3) High permeability ST-52 steel casing.*

The flow of current through the coils heats up the whole system. As the temperature of the structure rises, two main characteristics are affected. First, the conductivity of the copper decreases, and thus, maintaining the current requires more power. At the same time, the increase in temperature in the steel casing reduces its saturation magnetization. This, at the same time, reduces the magnetic flux density at the saturation condition ($B_s = \mu_0[M_s + H]$) [21].

These effects make necessary to include a refrigeration system for the solenoids. That is achieved with the division into sub-coils, which allows the solenoid to conduct heat

through the material in between sub-coils to the exterior. In addition, a water refrigerating system is included through the steel casing.

Magnetic flux density field

The magnetic field of the solenoid is plotted along the axis, for the different computation methods, in Figure 15. The main difference between the calculation in Ansys AIM and SIMION, is that the first allows to introduce the B-H curve for the ST-52 steel casing, that is, $\mu_r(H)$ (relative magnetic permeability), whereas SIMION only supports a constant μ_r. However, this should not introduce a big difference as long as the material stays in the linear region, that is, below the saturation level of the steel. This is confirmed in Figure 15, where it can be seen that the calculations in SIMION and Ansys AIM are very similar. On the other hand, we can appreciate how the experimental data differs substantially from the predicted magnetic flux density module in the designed solenoid. This difference is due to a flaw in the manufacturing of the solenoids, which was found after their characterization[5]. The fault is that the steel casing had the caps at both sides of the solenoid built from aluminium ($\mu_r(Al) \simeq 1$) [22] instead of magnetic steel, making the confinement very poor. This results, as can be seen in Figure 15, in a magnetic field that extends further and is weaker in the center of the solenoid.

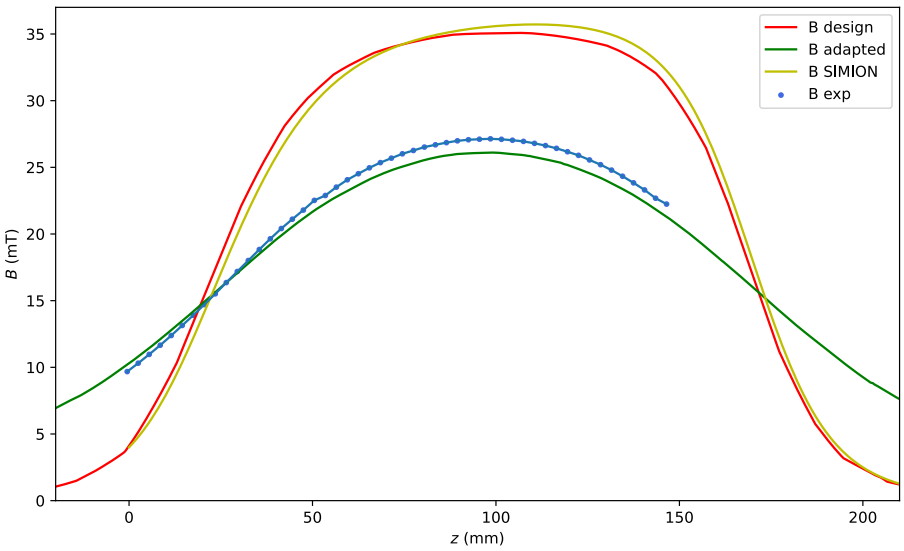

Figure 15: *Magnetic flux density module profile along the magnetic axis of the solenoid. Four curves are shown: the simulation in SIMION, the experimental data, the simulation in Ansys AIM of the designed solenoid and an simulation of an adapted design to match the experimental data. The uncertainty in the measured data is 0.05 mT. Position $z = 0$ marks the start of the solenoid.*

[5]The magnetic characterization was performed in a parallel project. A magnetic flux density mapping of the solenoids was carried out with a 3 axis Hall sensor attached to a computer controlled XYZ positioner. The most characteristic representation of the field is its module along the central axis.

The manufacturing flaw will have to be fixed, but we will still analyse the dynamics of the beam with the corresponding magnetic flux density field. Through that simulations it will be learnt how a bad confining of the field affects the the focusing of the beam.

5.2 Characterization of the beam at the LEBT inlet

5.2.1 Particle group definition

Once the systems geometry and the electrostatic/magnetic fields are generated inside SIMION's workbench, the next step is to define the group of particles that conform the ion beam. The group of particles needs to be representative of the protons generated in the ion source. Also, the number of particles has to be large enough in order to give statistically meaningful results. This value is found to be 40,000 particles, it will be justified later in this section, when we compute the emittance of the beam at the LEBT inlet.

The particles will be spatially set in a Gaussian distribution with standard deviation of $\sigma_{x,y} = 0.55$ mm. The parameters defined are set in order to maximize the number of particles that get through the Einzel lens. If, for example, a wider Gaussian were arranged, many of the particles would splat against the electrodes. This would result in a greater computational cost and no additional information about the system's characteristics. The velocity is set as unidirectional along the z axis with an energy of 2 eV, enough to get the beam moving through the extraction electrode, but insignificant compared with the 30 KeV they attain afterwards[6]. Mass and charge are set to be those of the proton.

5.2.2 Measurements of beam radius, trace-space diagram and emittance

This characterization is useful for various reasons. First, it allows to save an ION file [6], which contains the positions and velocities of the particles for the z coordinate at the entry of the LEBT. This file will, in the latter simulations, be the initial particle distribution. With this approach, the calculation of the potential array corresponding to the extraction electrode and Einzel lens, and the tracing of the trajectories of the 40,000 particles, is not needed in the preceding simulations. Said approach makes this study less time consuming[7].

On the other hand, the results obtained for the beam characteristics before entering the LEBT allow, through comparison, to study the contribution of the LEBT to the focusing and emittance growth (if it existed). The results are shown in Figures 16, 17 and 18.

Figure 16 presents the profile of the beam at the extraction system, where it can be seen how the beam is very parallel at the entrance of the LEBT. Then, Figure 17 shows how the particles follow a gaussian distribution, with an increase in the number of particles in the rim of the beam. This effect is due to a collimation performed in the

[6]A more realistic definition would be to give the particles the Maxwell velocity distribution [23], characteristic of a particle gas with a given temperature. This could have been implemented through a user program, but is left for a future project.

[7]These computations can take up to 8 hours in a 12 i9 core and 64GB RAM computer. The particle trajectory tracing can be parallelized, but the fields computation can not.

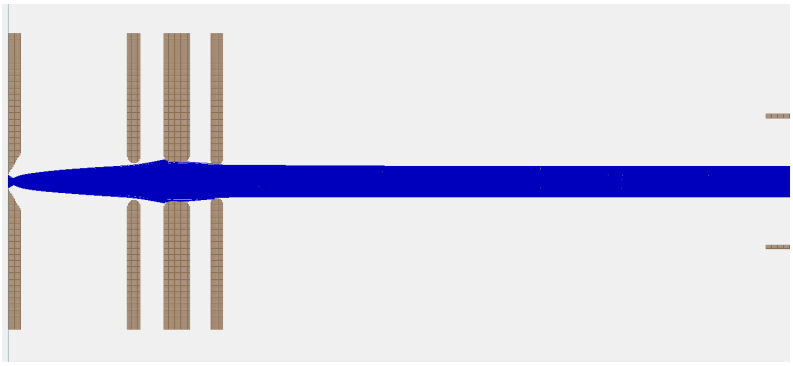

Figure 16: *Representation of the trajectories of the protons traveling through the extraction electrode and Einzel lens. It can bee seen how some particles splat against the central electrode of the lens. The beam seems to enter the LEBT as a cold beam (no transversal velocities).*

Einzel lens. The particles that travel near the electrodes bend their trajectories more abruptly. When the ions travel near the sources of the electrostatic fields, the paraxial approximation is no longer valid and more terms of the potential in (3.8) would need to be taken into account. This is a non-linear effect, the paraxial approximation is not valid for the ions that travel near the sources of the electrostatic fields.

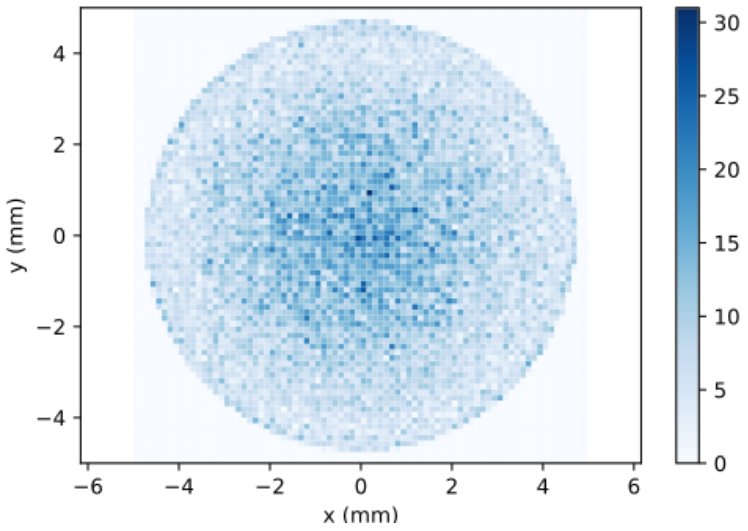

Figure 17: *Histogram of the number of particles at the entry of the LEBT. The distribution is gaussian-like, with a slight increase in the rim. This effect could be a collimation performed by the Einzel lens. The radius of the beam is 4.7 mm.*

Figure 18 is the trace-space diagram, which shows the divergence of the beam in this section of the accelerator. However, as was seen in Figure 16, the angle deviations are low, of order of mrad. The curved region in the extremes of the trace-diagram corresponds to the non-linear effect mentioned before. These effects lead to RMS emittance growth [10], but can be avoided by extracting the protons of the rim by means of a, for example, 3.5 mm radius aperture. Reducing the emittance through this method increases the quality of the beam, but reduces its intensity.

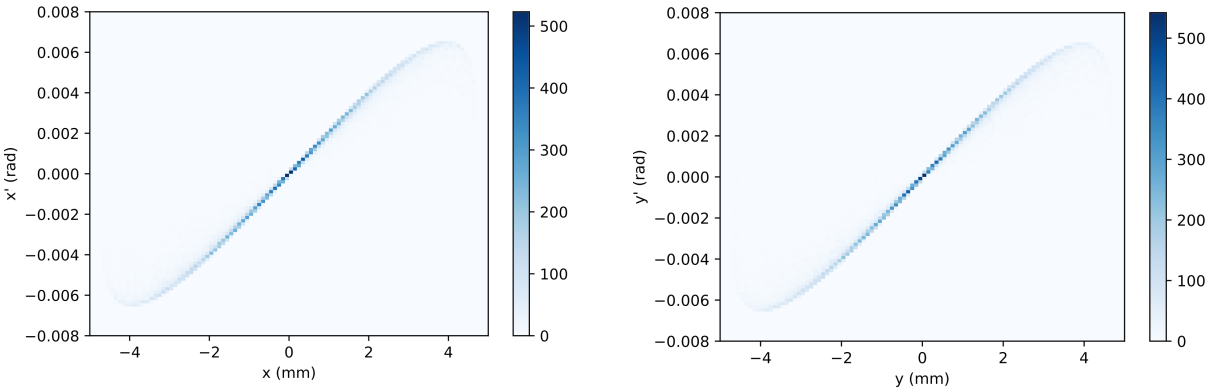

Figure 18: *Trace-space diagrams for the x and y axes. It can be seen how the beam is divergent. The particles in the positive positions have positive slope (x' or y') and the particles in the negative positions have negative slope. Both trace-space diagrams are very similar and convey the same information. This is due to the cylindrical symmetry of the system. Here it can be seen that the beam is indeed cold; the maximum divergence is of units of mrads.*

In Figure 19 it is shown how the number of particles in the beam and the emittance decrease as the radius of an aperture situated at the entry of the LEBT decreases. At a value of approximately 2.9 mm, the emittance has decreased more than 90 %, but the number of particles has also decreased to 50 %. It is a design matter to decide whether or not the increase in the quality of the beam is more important than preserving the intensity.

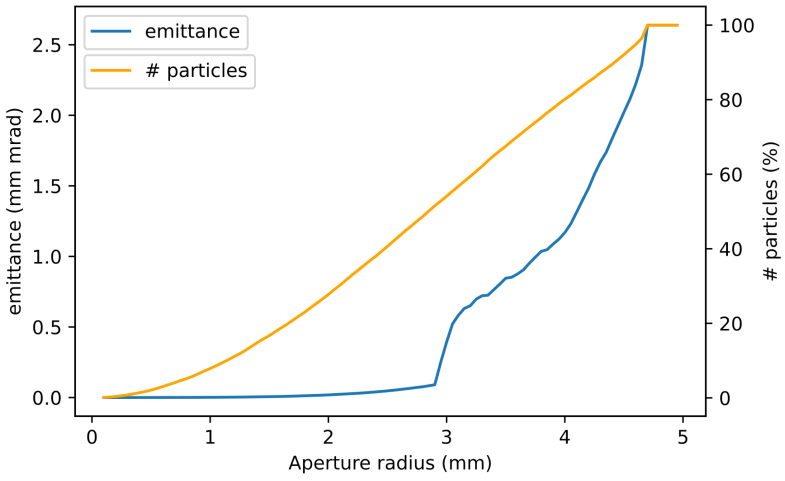

Figure 19: *Reduction of the emittance by means of an aperture of variable radius. It is also shown how the number of particles is consequently reduced.*

Finally, Table 1 presents the results for the emittances of the beam at the entry of the LEBT. To justify that 40,000 particles are enough to reproduce realistic results, we examine the difference between the emittance in the x and y axes. Due to the rotational symmetry, the x and y axis are completely equivalent; the emittance should be the same in both of them. From Table 1 it can be seen how increasing the number of particles reduces the distance between xx' and yy' emittances. The choice of 40,000 ions gives an adequate balance between low distance and manageable simulation time cost. In [24,25], emittances

of the order of 0.4 mm mrad (RMS normalized) are reported. This values, however, are given for higher currents than what Linac-7 will work with[8]. As the emittances shown in Table 1 are one order lower, we conclude, in absence of experimental evidence, that the quality of the beam is adequate for the RFQ.

Table 1: *Results at the entry of the LEBT of emittance and normalized emittance, for the x and y axes, for two simulations differentiated in the number of particles generated. Emittance units in mm mrad. The difference in emittance in the x and y axes ($\Delta E_{xx',rms} E_{yy',rms}$) is also calculated, the absolute value and the value relative to $E_{xx',rms}$ in %.*

N particles	$E_{xx',rms}$	$E^N_{xx',rms}$	$E_{yy',rms}$	$E^N_{yy',rms}$	$\Delta E_{xx'rms} E_{yy',rms}$
10,000	2.585	0.0205	2.525	0.0200	0.060 (2.32 %)
40,000	2.639	0.0209	2.626	0.0208	0.013 (0.49 %)

5.3 Characterization of the beam at the LEBT outlet

From the previous characterization of the beam at the LEBT inlet we now have the ION file which determines the positions and velocities of the ions at that position, at the entry of the LEBT. Then, for the following simulations we can subtract the extraction electrode and the Einzel lens from the workbench. The subsequent results will show how the beam characteristics change after traveling through the LEBT. Only a bad design of the LEBT would lead to emittance growth, so it is expected that it remains constant. The radius of the beam should decrease; how much will depend on the intensity set in the accelerators. It has been found that a current of 4.8 A in the first solenoid is enough to counter the divergence of the beam after the Einzel lens. Then, a current of 8 A focuses the beam to match the specifications of the RFQ, a beam diameter lower than 4 mm.

We will analyse 5 different cases, which differ in the computing software (SIMION or Ansys AIM), and the model of the solenoid (the designed solenoids or the experimentally measured solenoids).

1. **Ansys AIM, experimental 8 A.** Model in Ansys AIM that matches the experimentally measured field with a current of 4.8 A in sol. 1 and -8 A in sol. 2.

2. **Ansys AIM, experimental 9 A.** Model in Ansys AIM that matches the experimentally measured field with a current of 4.8 A in sol. 1 and -9 A in sol. 2.

3. **SIMION, experimental.** Model in SIMION that matches the experimentally measured field with a current of 4.8 A in sol. 1 and 8 A in sol. 2.

4. **Ansys AIM, design.** Model in Ansys AIM that matches the designed solenoids with a current of 4.8 A in sol. 1 and -8 A in sol. 2.

[8]Linac-7 is a low intensity linear accelerator with currents of tens of μA. The accelerators in [24, 25] report currents in the range of 3 mA to 18 mA

5. **SIMION, design.** Model in SIMION that matches the designed solenoids with a current of 4.8 A in sol. 1 and -8 A in sol. 2.

Notice that, in most cases, the first solenoid's current is opposite to that of the second. Publications [26] and [27] make reference to the convenience of introducing opposite currents in the solenoid pair to compensate tangential velocities in the plane normal to the propagation axis, uncoupling both directions (x and y). This will be the approach adopted in the Linac-7 project.

5.3.1 Experimental fields

To start with, we shall explain in detail the process the experimental data undergoes from the solenoid characterization to its introduction in SIMION. The experimental data does not form a uniform cubic mesh, a requirement from SIMION. Also, the experimental data were taken for a certain current (1 A) which does not match the ones used for the actual focusing of the beam. The approach, then, is to find a model of the solenoid that matches the collected data. This is done in Ansys AIM, and the model was found to be the designed model, but with a manufacturing flaw (the soft magnetic steel caps were made from aluminium). Magnetic flux density field maps (B maps) were then generated for 4.8, 8 and 9 A. The mesh generated in Ansys AIM is not uniform nor cubic. That B maps were then introduced in Matlab, and interpolated through the function *scatteredInterpolant* with a Natural Neighbour Interpolation method [28]. For a first approximation, a cubic grid with 1 mm distance between points is taken[9]. On the other hand, in order to calculate the B map in SIMION we introduce the same solenoid model in the software. The cubic grid in SIMION is defined through the Potential Arrays in which the field will be contained, the granularity is set to 0.1 mm[10].

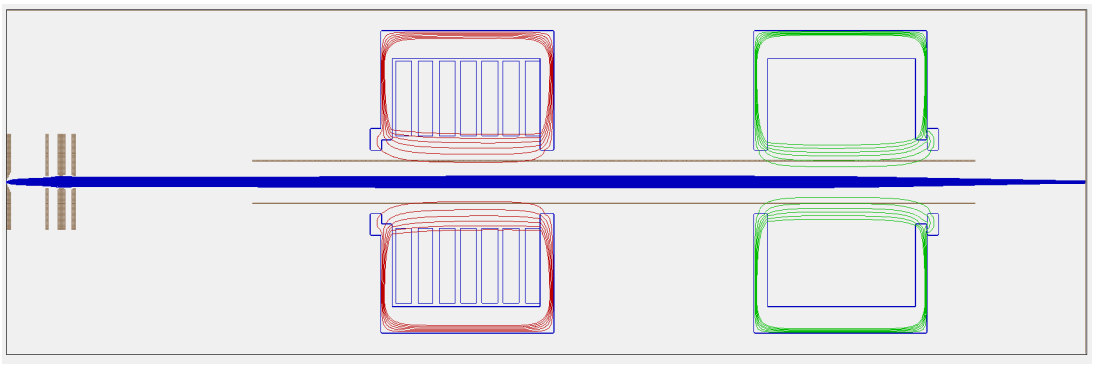

Figure 20: *Visualization of the beam traveling through the whole system: extraction, focusing and transport.*

Once the fields are computed and introduced in SIMION, the trajectories of the protons are simulated (Figure 20) parting from the results of Section 5.2. The beam is analysed at the outlet of the LEBT, in the position where a pepper-pot diagnostic is installed. The

[9]Notice that the number of points in a cubic mesh increases with the third power of that distance. A distance of 0.1 mm would imply 1,000 more points, and files 1,000 times heavier.

[10]In this case the size of the files is not so important, because they are completely managed by SIMION. They need no post-processing.

results for cases 1-3 are shown in Figure 21, and numerical results of emittance and radius of the beam are given in Table 2. The first characteristic to be noticed is that in this section of the accelerator the beam is convergent. The density of the particles has been compacted and, through comparison with Figure 17, has evolved increasing significantly the density of the particles in the rim of the beam. In terms of focusing, Ansys AIM predicts, for a current of 8 A, a ∼2 mm wider beam than the SIMION computed field. The origin of this difference is a truncation in Ansys AIM's generated field. The experimental field, due to the bad confinement, has a non-negligible contribution in the region between both solenoids, the exit of the Einzel lens and the entrance of the RFQ. That contribution can not be computed in Ansys AIM, because the academic license limits the mesh size available for simulation. From these three computations, then, the most accurate is the computation through SIMION; its field has been computed adding up the fields along the whole trajectory of the beam.

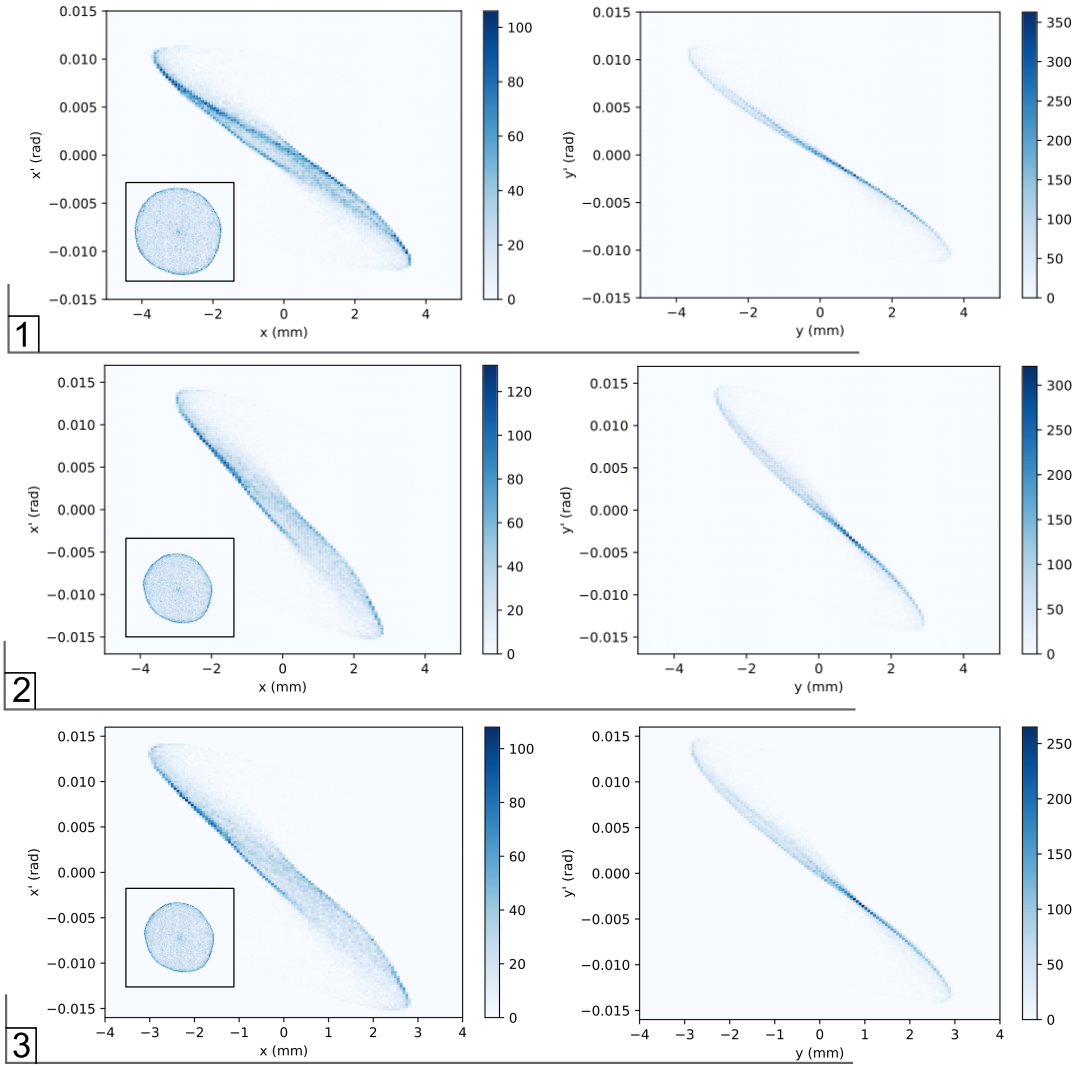

Figure 21: *Trace-space diagrams for the experimentally measured solenoids (cases 1-3) at the LEBT outlet. Convergent beam in all cases; most of the particles are in quadrants II and IV. The cylindrical symmetry has been lost in cases 1 and 2 (Ansys AIM). Corner of the xx' trace-space diagrams: density of particles at LEBT outlet.*

With regard to the emittances, the three simulations report similar results, in average the emittance in the x axis has increased 0.1 mm mrad and the y axis 0.6 mm mrad (3.8 % and 23.1 % respectively). The beam does not meet the requirement of focusing (2 mm).

An unexpected result from these simulations is that the cylindrical symmetry has been broken, the xx' and yy' trace-apace diagrams are no longer equal. This effect has its origin in the calculation of the trajectories through the extraction system and the grid of the Ansys AIM computed field. Though not appreciable in Figure 18, the beam is not completely symmetric with respect to the origin. The asymmetry at the start of the trajectories, howbeit small, impacts the subsequent dynamics of the beam.

5.3.2 Designed fields

The B map generated in Ansys AIM is introduced in SIMION through the same process as in the previous section. The main difference, which can be seen in Figure 15, is that the fields of the designed system are properly confined and, thus, no truncation is needed. The field is negligible in the region of the extraction system and in the entrance of the RFQ.

The results are shown in Figure 22. The principal difference when compared to the experimental field is the focusing. The radius of the beam with these fields (Table 2) fulfills the requirement of the RFQ. As before, the beam is convergent after traveling through the LEBT.

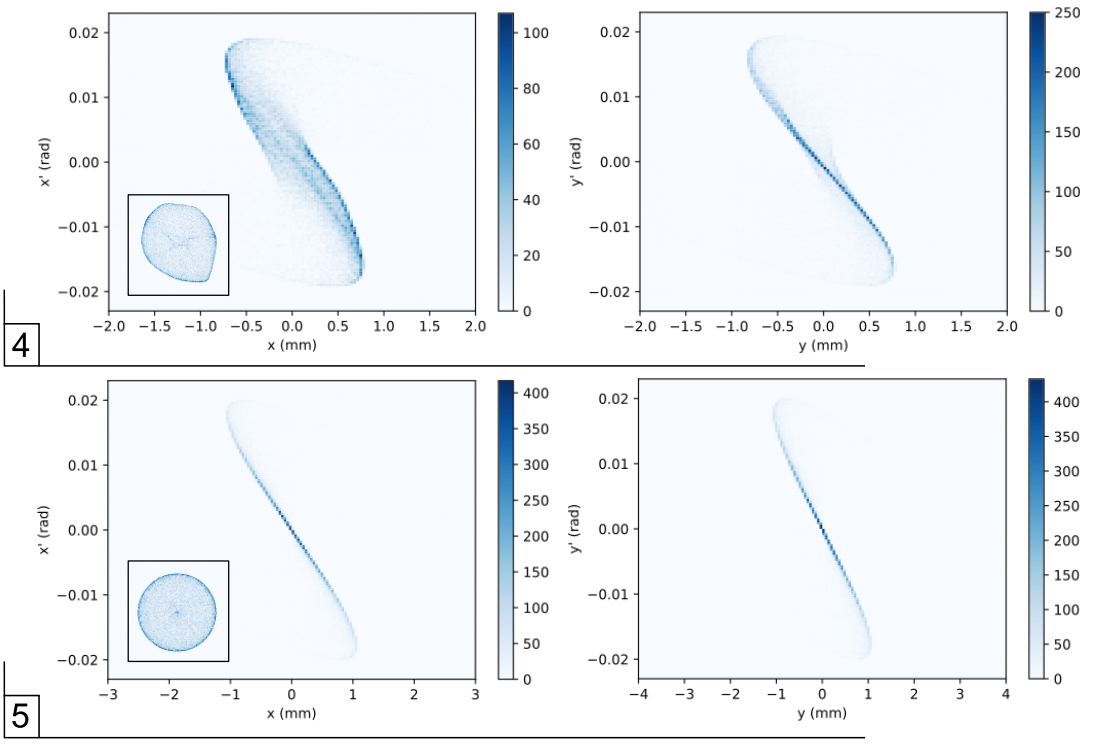

Figure 22: *Trace-space diagrams for the designed solenoids (cases 4-5) at the LEBT outlet. It can be seen how the beam is convergent, most of the particles are in quadrants II and IV. The cylindrical symmetry has been lost in case 4, simulated with the Ansys AIM computed field. Corner of the xx' trace-space diagrams: density of particles at LEBT outlet.*

Simulations with the Ansys AIM and SIMION computed fields differ mainly in the symmetry. The beam density in case 5 maintains the same distribution as in the LEBT inlet, but focused, convergent and with higher density in the rim. Conversely, the beam in case 4 is amorphous, though with similar characteristics of emittance and focusing. That difference could be due to numerical errors in the interpolation process. In principle, there is no fundamental reason for such asymmetries to appear, so the results found in case 5 are the ones expected to be the most realistic.

Table 2: *Results at the LEBT outlet of emittance and normalized emittance, for the x and y axes, for 5 simulations differentiated by the computed magnetic field of the solenoids. They are calculated in Ansys AIM or SIMION, according to the geometry of the design or adapted to match the experimental measurements of the fields. Emittance units in mm mrad.*

Magnetic Field	$E_{xx',rms}$	$E^N_{xx',rms}$	$E_{yy',rms}$	$E^N_{yy',rms}$	Radius (mm)
Ansys AIM, experimental 8A	2.7	0.021	3.1	0.024	3.6
Ansys AIM, experimental 9A	2.7	0.022	3.3	0.026	3.0
SIMION, experimental	2.7	0.022	3.3	0.026	2.9
Ansys AIM, design	2.7	0.021	2.9	0.023	0.8
SIMION, design	2.6	0.020	2.6	0.021	1.1

Through this analysis of the beam dynamics, the following conclusions can be extracted.

1. A correct confining of the magnetic field of the solenoids is a preferable to fulfill the beam requirements of entrance to the RFQ. Without confining higher currents would be needed.

2. The method of introducing the magnetic flux density field of the solenoids computed in Ansys, with the described method and a precision of 1mm, introduces dynamics which are uncharacteristic of the system. The numerical results are similar to those computed through SIMION only, with slightly greater values of emittance.

3. The simulation performed for case 5 confirms that the constructed LEBT is capable, pending experimental results, of introducing a convergent proton beam with a radius of 1.1mm and normalized RMS emittance of 0.02mm mrad.

Note about the code: *The following link refers to a GitHub repository where some of the code used to perform these simulations is available:* https://github.com/abermejillo/BachelorThesis/tree/main/Physics

6 Experimental validation of the LEBT's focusing

In this section, an experimental measurement of the focusing of the beam is presented. The obtained results are compared with those of a simulation, to partially validate the study we have performed through simulation.

The extraction system is not yet fully operational. It is not aligned with the beam tube, and due to imperfections in the surface of the electrodes, electric arcs appear when the voltage is increased. These arcs discharge the high voltage electrodes and, thus, the electric fields are unstable. Even though the experimental conditions are not optimal, with a low voltage in the extraction electrode some conclusions can be extracted.

The experimental setup is as follows. A voltage of 8 KV is set in the extraction electrode (4 KV in the central electrode of the Einzel lens), the highest voltage for which the voltage arcs do not perturb the system continuously. Then, the current in the first solenoid is set from 0 to 8 A in steps of 1 A. The beam travels through a slitted pepper-pot mask, reaches a phosphorescent screen and the image is sent through a mirror into a CCD. The result of this process can be seen in Figures 23a and 23b.

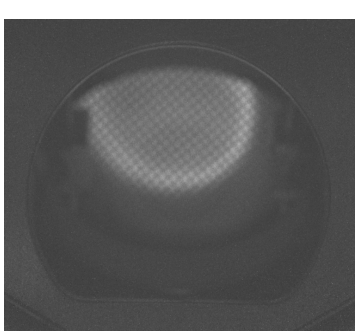

(a) *Image of an 8KeV beam spot on a phosphorescent screen for a current in solenoid 1 of 2A. The broad circle in which the beam is reflected is a 40mm diameter mirror.*

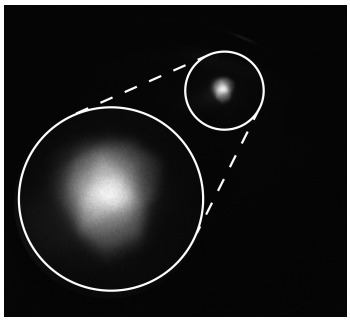

(b) *Image of an 8KeV beam spot on a phosphorescent screen for a current in solenoid 1 of 8A. Same scale as in Figure 23a, augmented section is included for greater detail.*

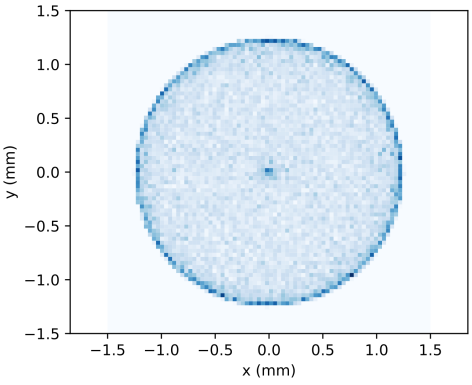

(c) *Histogram of the number of particles for an 8KeV beam. The radius of the beam is 1.22mm.*

Figure 23: *Beam focusing at the pepper-pot diagnostics position between the two solenoids of the LEBT.*

We want to compare the measured radius with a simulated value[11]. The simulated result (Figure 23c) is 1.22 mm. In order to extract the radius of the beam from the picture a 2D-gaussian fit is made of Figure 23b. That picture can be translated into a matrix, each pixel has assigned a value of light intensity, which relates to beam density, or number of protons that have collided in that spot of the phosphorescent screen. The gaussian fit is shown in Figure 24. The significant values of the gaussian fit are the standard deviations for the x and y axis: $\sigma_x = 25.4$ and $\sigma_y = 28.5$ (pixels). A common approach in accelerator physics is to take as the significant statistical value 2σ [8, 11], which takes into account

[11]The simulation was performed as described in Section 5.3.1, specifically as in case 3, the magnetic flux density field is computed through SIMION.

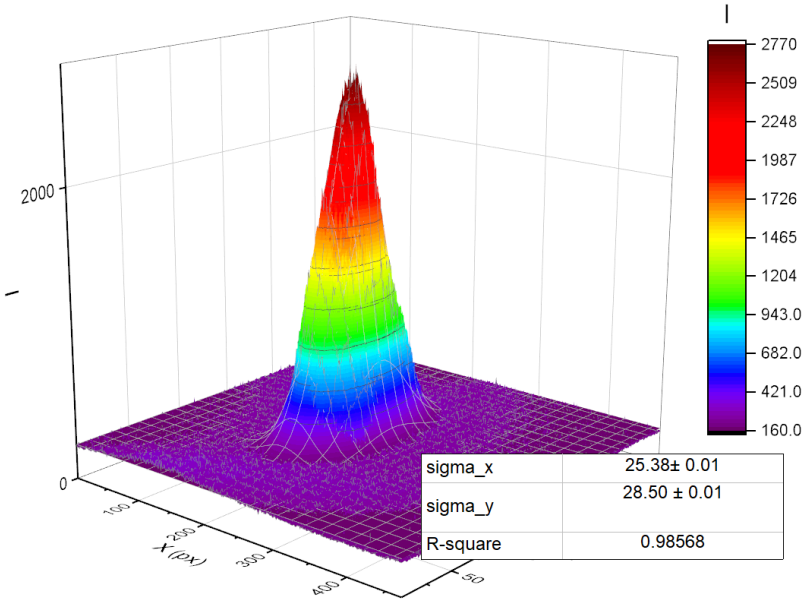

Figure 24: *Two dimensional gaussian fit of the beam spot image show in Figure 23b. Relevant parameters:* $\sigma_x = 25.38\ px$, $\sigma_y = 28.50\ px$, $R^2 = 0.98$.

$\sim$95 % of the particles. The calculated for σ_x and σ_y are given in pixels. The ImageJ [29] software allows to establish the relationship between pixels and distance through a known distance. That is made for Figure 23a for which the diameter of the mirror is known. Finally, the experimental radius extracted from the mean of both standard deviations is

$$\text{Experimental beam radius} \equiv 2\sigma = 1.36\ mm$$

Considering that the system is not aligned with the LEBT, the results are very similar. We have been able to predict through simulation a value (1.22 mm) with 10 % relative error. Taking into account that the objective is to fit the beam into a 2 mm radius aperture, that uncertainty of 0.14 mm is acceptable in order to be able to select a correct configuration of the LEBT's currents.

7 Conclusions

This project has consisted of a simulation study of the injector a linear particle accelerator, the Linac-7. The injector is formed by an extraction system and a magnetic LEBT, which is studied with special emphasis. The most relevant aspects and results of this process are enunciated hereafter.

The first sections serve as an introduction to accelerator physics. We defined some characteristics of an ion beam: intensity, trace-space diagrams and emittance. Then, we described the matrix formalism of ion optics. Deriving and solving the paraxial equation, we obtained an analytical process from which the trajectory of a particle traveling through electrostatic and magnetic lenses can be studied. In particular, it provides an intuitive understanding of the dynamics of a beam for two cases: the Einzel lens and the solenoid.

In order to obtain accurate results from the dynamics of a proton beam, simulations are indispensable. The paraxial equation discussed in Section 3 is limited due to the approximations made to derive it. Therefore, we learnt to set up and extract results from SIMION, an ion optics simulator. A brief introduction about its functioning was given and, then, we performed simple simulations in order to get familiarized and check the theoretical result of the focal length of a thin solenoid. The validation was successful, finding, for a given solenoid, a theoretical value of 0.902 mm and a simulation value of 0.918 mm. However, it was seen how, even in a simple case, the analytical formula yields a different result from the more accurate simulation result. This reflects the usefulness of computer simulations.

The main objective of this project has been the study of Linac-7's LEBT. We performed simulations of the trajectories of 40,000 protons traveling through the magnetic field generated by the LEBT's solenoids, which have been computed through two softwares: Ansys AIM and SIMION. The Ansys AIM computed fields were interpolated into a cubic grid with 1 mm spacing, which was found to be inaccurate. Figure 21 (1-2) and Figure 22 (1) manifest how the cylindrical symmetry of the system is not mirrored in the dynamics. On the other hand, through SIMION we utilized a 0.1 mm grid, which, as seen in Figure 22 (2), provided results that respect the symmetries of the system. Through this study it was also proven how a bad confining of the magnetic field is prejudicial for the performance of the LEBT. As seen in Table 2, for equal currents in the solenoids the focusing is three times weaker.

Finally, experimental measurements of the radius of the beam for a given configuration were compared with the simulation results. The experimentally measured radius was 1.36 mm and the simulated radius gave a more optimistic value of 1.22 mm.

This project has, then, fulfilled its objectives. We have learnt to perform ion optics simulations in SIMION, generating magnetic fields through user programming and introducing them from an external software, Ansys AIM. Through those simulations, it has been corroborated that the injector designed and manufactured for the Linac-7 is, pending further experimental confirmation, capable of introducing a proton beam with radius lower than 2 mm and normalized RMS emittance of 0.02 mm mrad.

7.1 Future work

Performing accurate and representative simulations can be a challenging task. Only experimental validation of the results is a guarantee that the system performs as predicted. However, some efforts can be made to increase the simulations' reliability. Some proposals are presented hereunder:

1. Introduce slight perturbations in the system, such as missalignment of the solenoids. By analysing how these changes affect the beam dynamics, we can study the robustness of the system.

2. Perform a study with different initial ion position and velocity distributions. For example, the Maxwell distribution has been proposed in Section 5.2.

3. Double check the results with other simulation programs. This project has done it by introducing the magnetic field from Ansys AIM into SIMION. The method, though, can be improved and retried with greater accuracy, for example, reducing the grid to match that used in SIMION.

Nevertheless, as said before, only through experimental measurements from the beam will we be certain that the constructed LEBT satisfies the RFQ's requirements. In order to obtain that confirmation, experimental tests will be carried out. Once the Einzel lens is fully operational and aligned, the beam will be characterized through the diagnostic elements installed between and after the solenoids. The experimental measurements of intensity, radius and emittance of the beam will be the conclusive test of the LEBT's performance.

References

[1] Andrew Sessler and Edmund Wilson, *Engines Of Discovery: A Century Of Particle Accelerators*. Wspc, (2007).

[2] Suzie Sheehy. (2018). "Applications of Accelerators". *Lectures of the CAS-CERN Accelerator School: Introduction to accelerator physics*. Accessed: June 15, 2021. [PowerPoint Slides]. Available: https://indico.cern.ch/event/685255/timetable/

[3] F. Hinterberger, "Lectures of the CAS-CERN Accelerator School: Ion optics with electrostatic lenses." Helmhols-Institut, Univ. of Bonn, Germany, (2006).

[4] Meusel, O and Bechtold, A and Pozimski, J and Ratzinger, U and Schempp, A and Klein, H, "Low-energy beam transport using space-charge lenses." *Nuclear Instruments and Methods in Physics Research Section A: Accelerators, Spectrometers, Detectors and Associated Equipment*, **544**(1–2), (2005).

[5] L. R. Prost, "Selected List of Low Energy Beam Transport Facilities for Light-Ion, High-Intensity Accelerators." arXiv preprint arXiv:1602.05488. (2016).

[6] D. Manura, D. Dahl (2008) *SIMION (R) 8.1 User Manual.* Adaptas Solutions, LLC, Palmer, MA 01069. Accessed: June 15, 2021. [Online]. Available: http://simion.com/manual/

[7] ANSYS, Inc. (1979). Ansys AIM. Accessed: June 15, 2021. [Online]. Available: https://www.ansys.com/

[8] Thomas P. Wagner, *RF linear accelerators.* John Wiley & Sons; Second revised edition, (2008).

[9] Brown,K. L. and Tautfest,G. W., "Faraday-Cup Monitors for High-Energy Electron Beams." *Review of Scientific Instruments*, **27**(9), 696-702, (1956).

[10] Martin, Reiser, *Theory and Design of Charged Particle Beams.* Wiley VCH, Second edition, (2008).

[11] R. Becker, W. B. Herrmannsfeldt, "Why π and mrad." *Rev. Sci. Instrum.* **77**, 03B907, (2005).

[12] J.G. Wang, D.X. Wang, M. Reiser, "Beam emittance measurement by the pepper-pot method." *Nuclear Instruments and Methods in Physics Research Section A: Accelerators, Spectrometers, Detectors and Associated Equipment*, **307**(2-3), 190-194, (1991).

[13] W.T. Weng, S.R. Mane, *Fundamentals of particle beam dynamics and phase space.* Brookhaven National Laboratory Associated Universities, Inc., (1991).

[14] A.G.Ruggiero, "Are we beating Liouville's theorem?" *eConf* **C7803272**, 123. (1978).

[15] CERN. "CERN accelerating science". Accessed: June 15, 2021. [Online]. Available: https://home.cern/

[16] Kumar, Vinit, Understanding the focusing of charged particle beams in a solenoid magnetic field." *American Journal of Physics*, **77**, 737-741, (2009).

[17] A. El-Kareh, *Electron Beams, Lenses and Optics.* Academic press, (1970).

[18] PUC-Rio (1993). Lua programming language. Accessed: June 15, 2021. [Online]. Available: http://www.lua.org/

[19] Autodesk, Inc. (1982). Fusion360. Accessed: June 15, 2021. [Online]. Available: https://www.autodesk.es/products/fusion-360

[20] Steven M. Lund, Yue Hao. (2018). *Accelerator Physics.* Accessed: June 16, 2021. [PowerPoint Slides]. Available: https://people.nscl.msu.edu/~lund/msu/phy905_2018/lec_lund/

[21] R. C. O'Handley, *Modern magnetic materials: Principles and applications.* John Wiley & Sons, Inc., Massachusetts Institute of Technology, (2000).

[22] Terry C. Edwards and Michael B. Steer. *Foundations for Microstrip Circuit Design. Apendix B.* John Wiley & Sons; Fourth Edition, (2016).

[23] J.C., Maxwell, "Illustrations of the dynamical theory of gases. Part I. On the motions and collisions of perfectly elastic spheres." *The London, Edinburgh, and Dublin Philosophical Magazine and Journal of Science*, 4th Series, **19**(125), 19-32, (1860).

[24] H. V. Smith, J. D. Schneider and R. Sheffield. Low-energy demonstration accelerator (LEDA) test results and plans. In PACS2001. Proceedings of the 2001 Particle Accelerator Conference (Cat. No. 01CH37268) **5**, 3296-3298. IEEE. (2001).

[25] J. H. Yoon, B. S. Lee, S. Choi, J. Y. Park, J. W. Ok and M. S. Won, "Development of compact linear accelerator in KBSI." *Review of Scientific Instruments* **83**, 02A315, (2012).

[26] J. Bahng, B. S. Lee, Y. Sato, J. W. Ok, J. Y. Park, J. H. Yoon, S. Choi, M.S. Won and E. S. Kim, "Development of a low-energy beam transport system at KBSI heavy-ion accelerator." *Nuclear Instruments and Methods in Physics Research Section A: Accelerators, Spectrometers, Detectors and Associated equipment*, **769**, 9-15, (2015).

[27] Y. Sato, M. Fujimaki, N. Fukunishi, A. Goto, Y. Higurashi, E. Ikezawa, O. Kamigaito, M. Kase, T. Nakagawa, J. Ohnishi, et al., "Design of the Low Energy Beam Transport in RIKEN new injector." IPAC 2010 - 1st International Particle Accelerator Conference, 01 (2010).

[28] Sibson, Robin, "A brief description of natural neighbor interpolation." In V. Barnett, Ed., Interpreting Multivariate Data. John Wiley & Sons, Inc., Ch 2, pp. 21–36, (1981).

[29] National Institutes of Health (1997). ImageJ. Accessed: June 15, 2021. [Online]. Available: https://imagej.nih.gov/ij